https://doi.org/10.5194/acp-2021-1074
Preprint. Discussion started: 9 February 2022

Atmospheric Chemistry and Physics Discussions

Kinetics of OH + SO_2 + M: Temperature-dependent rate coefficients in the fall-off regime and the influence of water vapour

Wenyu Sun,[1] Matias Berasategui,[1] Andrea Pozzer,[1] Jos lelieveld[1] and John N. Crowley[1]

Atmospheric Chemistry Department, Max-Planck-Institute for Chemistry, 55128 Mainz, Germany

Correspondence to: John N. Crowley (John.Crowley@mpic.de)

Abstract. The OH-initiated oxidation of SO_2 is the dominant, first step in the transformation of this atmospherically important trace-gas to particulate sulphate and accurate rate coefficients for the title reaction under all atmospheric conditions (pressures, temperatures and humidity) are required to assess its role in e.g. new particle formation. Prior to this study, no temperature dependent data were available in the fall-off regime for atmospherically relevant bath-gases. We thus address an important omission in the kinetic database for this reaction and highlight significant discrepancies in recommended parameterizations. In this work, generation of OH via pulsed laser photolysis at 248 and 351 nm was coupled to its detection by laser induced fluorescence to obtain rate coefficients (k_1) for the title reaction at pressures of 14−742 Torr and temperatures of 220−333 K in N_2 bath gas. In-situ SO_2 concentrations, central to accurate kinetic measurements under pseudo-first-order conditions, were measured by optical absorption. Under the conditions of the present study, the termolecular reaction between OH and SO_2 is in the fall-off regime and we parameterized the rate coefficients in N_2 in terms of low- ($k_{1,0}$) and high-pressure ($k_{1,\infty}$) limiting rate coefficients and a broadening factor (F_C) to obtain $k_{1,0}^{N2}$= 3.03×10^{-31} (T/300)$^{-4.10}$ cm^6 molecule^{-2} s^{-1}, $k_{1,\infty}$ = 2.00 ×10^{-12} cm^3 molecule^{-1} s^{-1}, and F_C = 0.58. The effects of water vapour on the title reaction were explored through measurements in N_2-H_2O mixtures at 273, 298 and 333 K using the same experimental methods. The rate coefficients are significantly enhanced by the presence of water vapour with $k_{1,0}^{H2O}$ = 1.65×10^{-30} cm^6 molecule^{-2} s^{-1}, which indicates that H_2O is a factor >5 more efficient in quenching the $HOSO_2$* association complex than N_2. A model-based comparison of our rate coefficients and parameterization with previous literature measurements and recommendations of evaluation panels are presented and discussed. The use of the new parameterization instead of the IUPAC or NASA evaluations, particularly after including H_2O as a third-body quencher, leads to a significant (10-30%) reduction in the lifetime of SO_2 in some parts of the atmosphere and increases the H_2SO_4 / SO_2 ratio concomitantly.

1 Introduction

Sulphur enters the atmosphere predominantly in the form of gaseous sulphur dioxide (SO_2) which results from both natural and anthropogenic sources (Stevenson et al., 2003). The amount of SO_2 produced from human activities, particularly via fossil fuel combustion, is similar to that resulting from natural emissions (e.g. volcanic eruptions), and can be dominant on a regional scale (Brown, 1982; Brimblecombe, 2013; Lelieveld et al., 1997). SO_2 is a key intermediate during the complex chemical and

https://doi.org/10.5194/acp-2021-1074
Preprint. Discussion started: 9 February 2022

Atmospheric Chemistry and Physics Discussions

photochemical reactions that ultimately transform reduced sulphur compounds to sulphates. The oxidation of SO_2 in the atmosphere occurs in the gas phase as well as in droplets and aerosol particles (Liu et al., 2020; Cox, 1979; Beilke and Gravenhorst, 1978). The gas-phase oxidation of SO_2 is initiated mainly by the OH radical (R1), with a small contribution in forested regions by stabilised Criegee intermediates (Mauldin Iii et al., 2012; Huang and Chao, 2015). Based on a seasonal, global average boundary layer OH concentration of 1×10^6 molecule cm^{-3} and the present recommendation for the rate coefficient (Atkinson et al., 2004; Iupac, 2021), the lifetime of SO_2 with respect to reaction with OH (to form $HOSO_2$) is a few days.

$$SO_2 + OH + M \rightarrow HOSO_2 + M \quad \text{(R1)}$$

Once collisionally stabilized $HOSO_2$ reacts with O_2 to form SO_3 (R2), which is hydrolysed to sulphuric acid (H_2SO_4) (R3).

$$HOSO_2 + O_2 \rightarrow HO_2 + SO_3 \quad \text{(R2)}$$

$$SO_3 + (H_2O)_n \rightarrow H_2SO_4 + (H_2O)_{n-1} \quad \text{(R3)}$$

H_2SO_4 can initiate particle formation (e.g. via reactions with basic trace-gases such as NH_3) or condense on existing particles, thus contributing to aerosol formation, growth and cloud droplet nucleation (Kulmala et al., 1998; Vehkamäki et al., 2002; Sipilä et al., 2010; Saltzman et al., 1983). The aforementioned processes occur throughout the atmosphere, affecting ecosystems as well as the earth troposphere radiation budget and thus climate (Badr and Probert, 1994; Lelieveld and Heintzenberg, 1992; Stevenson et al., 2003; Feichter et al., 1996). In addition, the oxidation of SO_2 to sulphate is a major sink of stratospheric OH and water (Bekki, 1995) and provides surface area for heterogeneous processes that e.g. contribute to stratospheric ozone depletion (Weisenstein et al., 1996; Heckendorn et al., 2009).

As a result of its central importance to atmospheric chemistry, the kinetics of the title reaction have been investigated in numerous experimental studies. The results of laboratory investigations of k_1, which serve as the basis for the IUPAC (Iupac, 2021) and NASA (Burkholder et al., 2020) evaluation panels, are summarized in **Table 1**. A few early measurements of k_1 at around 298 K and 1 atm N_2 (or air) (Izumi et al., 1984; Barnes et al., 1986; Davis et al., 1979; Castleman Jr and Tang, 1976; Cox and Sheppard, 1980) are not included in **Table 1**, as they do not contain information on the pressure- or temperature-dependence of the title reaction and display relatively large differences in k_1 at 298 K and 1 atm with values ranging from 5.99×10^{-13} to 1.22×10^{-12} cm^3 $molecule^{-1}$ s^{-1}. Surprisingly, for such an important reaction in atmospheric chemistry, no temperature-dependent measurements of k_1 in the fall-off regime have been carried out in atmospherically relevant bath gases (e.g. air or N_2) but in He for which the collision efficiency is much lower than for N_2 and O_2, the dominant components of the atmosphere. In addition, the latest measurements of k_1, (Blitz et al., 2017a) using modern, laser-based photolysis methods, suggest that previous measurements were strongly biased (to larger values) by the photo-excitation of SO_2 (see later).

The title reaction is in the fall-off regime across the temperature/pressure ranges in the atmosphere. To parameterize the rate coefficients for such reactions, the Troe-type formulation (Troe, 1983) is widely-used, which requires experimentally-determined high-pressure ($k_{1,\infty}$) and low-pressure ($k_{1,0}$) limiting rate coefficients as well as a broadening factor describing the transition at intermediate pressures. To date, the rate coefficient at the high-pressure limit has not been measured directly and the value of k_1 at 298 K of ~2.4×10^{-12} cm^3 $molecule^{-1}$ s^{-1} at 96 bar (72000 Torr) of He, the highest pressure explored to date, is

https://doi.org/10.5194/acp-2021-1074
Preprint. Discussion started: 9 February 2022

still below the extrapolated $k_{1,\infty}$ value of 3.6×10^{-12} cm^3 molecule^{-1} s^{-1} (Fulle et al., 1999). (Blitz et al., 2017a) derived values of $k_{1,\infty}$ indirectly via measurements of the vibrational relaxation of OH in collision with SO_2, but obtained a much lower value of $k_{1,\infty} = 7.2\times10^{-13}$ cm^3 molecule^{-1} s^{-1}. The value of $k_{1,\infty}$ presently recommended by IUPAC (last updated in November 2017) and NASA (last updated in May 2020) are 2.0×10^{-12} and 1.7×10^{-12} cm^3 molecule^{-1} s^{-1}, respectively, falling between those of (Fulle et al., 1999) and (Blitz et al., 2017a).

From the studies reporting low-pressure limiting rate coefficients, largely obtained in flow-tube experiments, it is unclear whether $k_{1,0}$ could be accurately derived through linear fitting to measured values of k_1 over a small pressure range, as measurements at the experimental pressures (a few Torr) were already impacted by fall-off. As discussed by Amedro et al. (2019), other factors such as wall-losses of OH add to the difficulty of deriving accurate low-pressure limiting rate coefficients in flow-tube experiments, especially at low temperatures.

Apart from N_2 and O_2, water vapour (H_2O) is a major atmospheric component. In particular, in the relatively warm boundary layer, e.g. in the tropics, the mixing ratio of water vapour can exceed 5%. For termolecular reactions involving OH, H_2O may be expected to be a more efficient third-body quenching agent than N_2 and O_2 (Troe, 2003; Amedro et al., 2020) and the presence of water vapour can significantly enhance rate coefficients of third-body reactions in the low-pressure and fall-off regimes. A recent study (Amedro et al., 2020) demonstrated that neglecting to consider the influence of water vapour would lead to an underestimation in the rate coefficients of the OH+NO_2 reaction by ~ 10% in some parts of the lower atmosphere. Given the similarities between the title reaction and the OH + NO_2 reaction, the participation of H_2O as a third-body quencher may also significantly enhance k_1, and such effects need to be examined experimentally.

The goals of this study were to address some of the shortcomings in the present dataset on the reaction of OH with SO_2 by accurately measuring k_1 in N_2 bath gas over a wide temperature/pressure range relevant for the atmosphere and to elucidate the role of water vapour as a third-body quencher on the title reaction. Such datasets are expected to yield a new parameterization for k_1 with reduced uncertainties.

2 Experimental methods

Rate coefficients for the title reaction were derived using the pulsed-laser-photolysis (PLP)-laser induced fluorescence (LIF) technique under pseudo-first-order conditions ([SO_2] >> [OH], see Section 3.2). The concentrations of SO_2, as well as H_2O in the experiments exploring the effect of water vapour, were obtained online via optical absorption measurements.

2.1 PLP-LIF technique

Detailed descriptions of the PLP-LIF setup are given in previous publications (Wollenhaupt et al., 2000; Amedro et al., 2019). Briefly, the reaction took place in a jacketed quartz reactor with a volume of ~500 cm^3, the temperature inside the reactor was regulated by circulating ethanol (at 220 K) or 60:40 ethylene glycol mixture (250, 273 and 333 K) through an outer jacket. The temperature at the centre of the reaction volume was monitored by a J-type thermocouple before and after each experiment;

https://doi.org/10.5194/acp-2021-1074
Preprint. Discussion started: 9 February 2022

Atmospheric Chemistry and Physics Discussions

the pressure was measured using 100 and 1000 Torr capacitance manometers. To ensure that a fresh gas sample was photolysed at each laser pulse (laser frequency: 10 Hz) and to avoid accumulation of products, the average linear-velocity of gas flowing through the reactor was kept at ~ 8−9 cm s^{-1} by adjusting the total volume flow rates according to the pressure and temperature in the reactor. For the vast majority of experiments, a KrF excimer laser (COMPex 205F, Coherent) provided pulses of 248 nm light (~20 ns) to photolyse H_2O_2 or HNO_3 for the generation of OH radicals in the vibrational ground-state (Schiffman et al., 1993).

$H_2O_2 + h\nu$ (248 nm) → 2 OH (R4)

$HNO_3 + h\nu$ (248 nm) → $OH + NO_2$ (R5)

In addition, a limited set of experiments were carried out in which HONO was photolysed at 351 nm (XeF excimer laser):

HONO + $h\nu$ (351 nm) → OH + NO (R6)

OH radicals thus generated were excited at 282 nm ($A^2\Sigma$ (v=1) ← $X^2\Pi$ (v=0)) by a YAG-pumped dye-laser and the subsequent OH fluorescence was detected by a photomultiplier placed behind a 309 nm interference filter and a BG 26 glass cut-off filter. The photolysis laser fluence was measured by a Joule-meter placed behind the exit window of the reactor, and the shot-to-shot variation in the intensity of the dye-laser was monitored by a photodiode. The timing between the triggers of the photolysis and probe lasers was scanned using a digital delay generator; time-dependent OH profiles were obtained by accumulating the fluorescence signals using a boxcar integrator. Fluorescence resulting from the excitation of SO_2 at 282 nm was also observed using this set-up, which results in a constant background signal during each experiment. Typically, 20 points were recorded before triggering the excimer laser to measure the background signal which also includes a component from electronic noise. The background signal was subtracted from the measured OH profile before further kinetic analyses.

2.2 On-line optical absorption measurements

The accurate determination of the rate coefficients under pseudo-first-order conditions requires reliable quantification of SO_2 concentrations ($[SO_2]$). In this work, online optical absorption cells were located both upstream and downstream of the reactor to monitor the SO_2 concentration at room temperature (298 K). Upstream of the reactor, light from a deuterium lamp was directed through a multi-pass absorption cell (l = 110 cm ×8 = 880 cm) and detected by a low resolution ($\Delta\lambda$ = 2 nm) spectrograph (Ocean-Optics USB 2000). The measured optical density over the wavelength range of 240−325 nm was fit to a reference spectrum (Manatt and Lane, 1993) to derive SO_2 concentrations. The second (downstream) optical absorption cell (l = 34.8 cm) was equipped with a low-pressure Zinc lamp and monitored optical density at 213.86 nm to measure the concentration of SO_2 (see Section 3.1) and the OH precursors H_2O_2 and HNO_3. SO_2 concentrations were calculated using a 213.86 nm cross-section derived in separate experiments (see later). Concentrations of H_2O_2 and HNO_3 were calculated using $\sigma_{213.86\,nm}$ (H_2O_2) = 3.30 × 10^{-19} (Vaghjiani and Ravishankara, 1989) and $\sigma_{213.86\,nm}$ (HNO_3) = 4.52 × 10^{-19} (Dulitz et al., 2018). Approximate, initial concentrations of OH radicals were calculated from the precursor concentrations and the excimer laser fluence as recorded by the Joule-meter. A third absorption cell (l = 40 cm, located downstream of the 213.86 nm cell) equipped

https://doi.org/10.5194/acp-2021-1074
Preprint. Discussion started: 9 February 2022

Atmospheric Chemistry and Physics Discussions

with a low-pressure 184.95 nm Hg lamp as light source was additionally used in the experiments exploring the impact of water vapour. In this case, a cross section of $\sigma_{184.95\,nm}$ (H_2O) = 7.14×10^{-20} (Cantrell et al., 1997) was used.

2.3. Chemicals

Nitrogen (N_2, 99.999 %) was supplied by Westfalen and used without further purification. SO_2 (Merck, 99.8%) was diluted in N_2 and stored in a stainless-steel cylinder. Hydrogen peroxide (H_2O_2, AppliChem, 35 %) was vacuum distilled to > 90 wt. % purity. Anhydrous HNO_3 was synthesized by mixing potassium nitrate (KNO_3, Sigma-Aldrich, 99%) and sulphuric acid (H_2SO_4, Roth, 98%), and condensing the HNO_3 vapour in a trap cooled with liquid nitrogen. Distilled water (Merck, liquid chromatography grade) was degassed before use.

3 Results and discussion

3.1. Quantification of SO_2 concentrations

SO_2 absorption spectra over 170−330 nm at room temperature are presented in **Fig. 1**, including a low-resolution ($\Delta\lambda$ = 0.1 nm) datasets reviewed and compiled by Manatt and Lane (1993) and a set of higher-resolution data ($\Delta\lambda$ = 2.5×10^{-4} nm) spanning 198−325 nm reported by Stark and co-workers (Stark et al., 1999; Rufus et al., 2003). The two absorption bands (240-330 nm and 170-230 nm) correspond to the $\tilde{B}(^1B_1) \leftarrow \tilde{X}(^1A_1)$ and the $\tilde{C}(^1B_2) \leftarrow \tilde{X}(^1A_1)$ transitions, respectively (Rollins et al., 2016). The high-resolution measurements by Stark et al. (1999) reveal very narrow rotational-vibrational lines in the 200−220 nm region, and cross-sections that are factors of 2-3 larger than those of Manatt and Lane (1993). Clearly, the use of an inappropriate cross section at the wavelength of our very narrow Zn-atomic emission line (~213.86 nm) could introduce large uncertainty in SO_2 concentration. For this reason, we derived an effective cross-section for our Zn-lamp emission by comparing absorption measurements in the multi-pass cell and the 213.86 nm cell for a flowing gas-mixture of SO_2 in N_2. We refer to this cross-section as an "effective" cross-section as nearby, weaker atomic lines will also pass through the interference filter (214 ± 5 nm) used to isolate the 213.86 nm line. In **Fig. 1**, broadband (240−325 nm, resolution ~ 2 nm) absorption measurements recorded using the multi-pass cell are compared to the reference spectrum of Manatt and Lane (1993). SO_2 concentrations were determined through least squares fitting the measured optical density to the reference spectrum degraded to the same resolution as our spectrometer. The effective cross section at 213.86 nm was then derived according to the Beer-Lambert law, taking into account pressure differences in the two absorption cells, as shown in **Fig. 2**. The slope of a linear regression through the data points is the effective cross-section of SO_2 at the emission wavelength of our low-pressure Zn-Lamp. The value obtained (4.00×10^{-18} cm^2 molecule^{-1}) is very close (within ~ 3 %) to the value of 4.07×10^{-18} cm^2 molecule^{-1} listed at 213.86 nm by Stark et al. (1999) and the value of 3.87×10^{-18} cm^2 molecule^{-1} derived by Wine et al. (1984) using a similar experimental setup. The high correlation coefficient (R^2 of 0.9984) for the linear regression of all data points obtained at different pressures (41 to 494 Torr) indicates that the effective value of $\sigma_{213.86}(SO_2)$ is independent of pressure. SO_2

https://doi.org/10.5194/acp-2021-1074
Preprint. Discussion started: 9 February 2022

Atmospheric Chemistry and Physics Discussions

concentration measurements using the two absorption cells in the experiments at different temperatures are plotted in **Fig. 3**. The good agreement (slope very close to 1) between the measured (at room temperature) SO_2 concentrations upstream and downstream of the reactor (held at temperatures between 220 and 333 K) shows that no SO_2 is lost in transit (e.g. via adsorption to surfaces or condensation) through the cold/hot reactor. The scatter in this plot is caused by small baseline shifts in the long path measurements upstream of the reactor.

3.2. Rate coefficients for the title reaction in N_2

Rate coefficients for the title reaction in N_2 bath were measured at pressures between 14 and 742 Torr at five different temperatures (220, 250, 273, 298 and 333 K). In deriving a parameterisation for the rate coefficient in air (see later), we assume that, as is the case for the vast majority of termolecular reactions, N_2 and O_2 (the major components of air) have the same collisional quenching efficiency. In all experiments, the initial OH concentration was kept sufficiently low (10^{11}–10^{12} molecule cm^{-3}) relative to that of SO_2 (6×10^{14} to 6×10^{15} molecule cm^{-3}) so that pseudo-first-order conditions applied and the decay of OH may be described by:

$$[OH]_t = [OH]_0(-k't) \quad (1)$$

where $[OH]_t$ is the OH concentration at time t after the photolysis laser pulse and k' is the pseudo-first-order rate coefficient defined as

$$k' = k_1[SO_2] + k_d \quad (2)$$

k_1 (in cm^3 $molecule^{-1}$ s^{-1}) is the bimolecular rate coefficient for the title reaction and k_d (in s^{-1}) accounts for the OH removal through reactions with H_2O_2 or HNO_3 (R7 or R8) as well as OH loss due to diffusion out of the reaction zone.

$$OH + H_2O_2 \rightarrow H_2O + HO_2 \quad (R7)$$

$$OH + HNO_3 \rightarrow H_2O + NO_3 \quad (R8)$$

Fig. 4 displays a set of OH decay profiles at six different SO_2 concentrations ranging from 0 to 5.34×10^{15} molecule cm^{-3} at 298 K in 59.9 Torr N_2. H_2O_2 was used as OH precursor in this dataset and the initial OH concentration was ~ 4×10^{11} molecule cm^{-3}. Each OH decay is the average of 20 measurements taken over a period of ~ 5 minutes. For each profile, the decay constant k' was obtained through least-squares fitting to Eq. (1). From each set of OH decays at a given temperature, pressure and bath-gas, the associated bimolecular rate coefficient k_1 was derived using Eq. (2) as shown in **Fig. 5** which plots k' against $[SO_2]$ at 298 K at four different pressures.

Previous experimental studies have reported that the photo-excitation of SO_2 can have a large impact on the kinetics of OH loss. To circumvent this, optical filters containing SO_2 have been used to reduce the absorption of e.g. light from flash-lamps (160-220 nm) (Paraskevopoulos et al., 1983; Wine et al., 1984). The 248 nm laser light used in the current set up is beyond the SO_2 photodissociation threshold of 219 nm so single-photon SO_2 photodissociation cannot affect the measurements for k_1. However, using a similar setup at 248 nm, (Blitz et al., 2017b, a) found evidence for two-photon dissociation of SO_2 in their experiments in He and reported a high-pressure limiting rate coefficient that is lower (by a factor of 2−5) than all other measurements or recommendations by evaluation panels. Blitz et al. (2017b) suggested that previous measurements were

https://doi.org/10.5194/acp-2021-1074
Preprint. Discussion started: 9 February 2022


Atmospheric Chemistry and Physics Discussions

biased by additional OH removal by radical-radical reactions initiated by the two-photon dissociation of SO_2. In order to evaluate whether SO_2 photoexcitation could have impacted on our measurements of k_1 in N_2, we conducted measurements at 298 K and 14 Torr in N_2 with the excimer laser power varied by a factor of ~14. Over this energy range, the impact of any two-photon processes would scale by a factor of ~ 200. k_1 was thus measured in a total of 10 experiments, for which SO_2 concentrations ranged from 1.2×10^{15} to 6.0×10^{15} molecule cm^{-3}, the concentration of H_2O_2 was kept at around 3×10^{14} molecule cm^{-3}, and the laser fluence was varied from ~0.5 to ~9.5 mJ cm^{-2}. Values of k_1 as a function of the 248 nm laser fluence are displayed in **Fig. 6**. Our data clearly show that k_1 is independent of laser fluence (the average value is $1.29 \pm 0.05 \times10^{-13}$ cm^3 $molecule^{-1}$ s^{-1}), suggesting that, under our experimental conditions in N_2 bath, secondary reactions between OH radicals resulting from the photoexcitation of SO_2 are insignificant. This observation helps to rule out that single- or two-photon processes involving SO_2 excitation or dissociation do not bias the OH decay and that reactions of OH with e.g. products of R1 (i.e. $HOSO_2$) or reaction with HO_2 and NO_3 (formed in R7 and R8) are unimportant. To examine the potential for two-photon photolysis of SO_2 in He bath-gas, we added H_2O to a reaction mixture of H_2O_2, SO_2 and He and observed non-exponential OH kinetics, suggesting the intermediacy of $O(^1D)$:

$$SO_2 + 2\,h\nu \rightarrow O(^1D) + SO \quad \text{(R9)}$$

$$O(^1D) + H_2O \rightarrow 2\,OH \quad \text{(R10)}$$

We emphasise that such effects were not seen in N_2 bath-gas in which $O(^1D)$ is rapidly quenched to less reactive $O(^3P)$.

To confirm beyond doubt that our measurements using 248 nm PLP are not biased by SO_2 excitation, an additional experiment was performed (193.2 Torr and 298 K) using HONO photolysis at 351 nm as OH precursor. At 351 nm the SO_2 absorption cross-section is ~ 3 orders of magnitude lower than at 248 nm and SO_2 excitation is negligible. HONO was generated in-situ by the dropwise addition of a 0.1 M $NaNO_2$ solution to a 20 wt. % H_2SO_4 solution and the characteristic bands at around 342, 354 and 368 nm (Stutz et al., 2000) were monitored by the multi-pass optical absorption cell. This setup provided sufficient amounts of HONO (~10^{14} molecule cm^{-3}) for kinetic measurements for about 1−1.5 hours after adding a few drops of the $NaNO_2$ solution. Note that the concentration of H_2O above the H_2SO_4 solution is very low, so that these can be considered to be dry experiments (i.e. in N_2 bath-gas).

Unlike the H_2O_2 and HNO_3 sources of OH described above, the concentration of HONO was not stable over the time required to measure a series of values of *k*' in the presence of various amounts of SO_2. Therefore, measurements of *k*' with and without SO_2 were conducted intermittently. **Fig. 7** displays the measured first-order OH decay rate constants (*k*') with different amounts of SO_2 present in the system and over a period of ~ 2.5 hours. In the absence of SO_2 (blue symbols), the *k*' decreased from an initial value of ~ 2800 s^{-1} to one of ~800 s^{-1} at 5200 s. This is mainly due to the reaction of OH with HONO and impurities such as NO_2 and NO. After ~5400 s a few drops of $NaNO_2$ were again added to the H_2SO_4 solution and the increase in [HONO] was accompanied by an increase in *k*'. The decay in *k*' over time was fit with a second-order polynomial function which, via interpolation, was used to calculate the contribution of OH loss in the absence of SO_2 (i.e. k_d) from the individual values obtained with SO_2 present. Based on the loss rate constants in the absence of SO_2 and the rate coefficient for reaction of OH

https://doi.org/10.5194/acp-2021-1074
Preprint. Discussion started: 9 February 2022

Atmospheric Chemistry and Physics Discussions

with HONO (k_{11} (298 K) = 6.0×10^{-12} $cm^3 molecule^{-1} s^{-1}$) (Atkinson et al., 2004), we estimate the HONO concentrations to be ~1−5×10^{14} molecule cm^{-3}. .

HONO + OH → NO_2 + H_2O (R11)

Combined with the photolysis laser fluence of around 1 mJ cm^{-2}, this results in an initial OH concentration of 0.3−1.5 $\times10^{11}$ molecule cm^{-3}. A total of five different SO_2 concentrations were used in these experiments, and at each SO_2 concentration the measurement of *k*' was repeated four times. The averaged values of *k*', after correction for the contribution from reactions of OH with HONO and other impurities as well as diffusion loss of OH, are plotted against SO_2 concentration in **Fig. 8**. A linear regression yields a value of k_1 = 4.91 ± 0.13 × 10^{-13} cm^3 $molecule^{-1}$ s^{-1}. A similar set of experiments at 273 K and 295 Torr yielded k_1 = 8.44 ± 0.19 × 10^{-13} cm^3 $molecule^{-1}$ s^{-1}. Owing to the more convoluted experimental procedure and data analysis and also the larger OH losses in the absence of SO_2, (up to ~3000 s^{-1}) the overall uncertainty of the rate coefficient obtained in this manner is larger than those obtained using H_2O_2 and HNO_3 as OH precursors and the difference (~10 %) between the rate constant obtained using the 248 nm photouch lysis of H_2O_2 or HNO_3 or HONO as OH source is not considered significant. In any case, this level of agreement (combined with the laser fluence variation described above) rules out a bias to k_1 of the magnitude reported by Blitz et al. (2017b) when working at 248 nm in N_2 bath-gas.

Our measurements of k_1 obtained in N_2 bath (in total > 100) are plotted against the N_2 concentration, at five different temperatures in **Fig. 9**. The rate coefficients and associated experimental conditions are listed in **Table S1** in the Supplementary Information**.** The rate coefficients obtained using H_2O_2 and HNO_3 as OH precursors (at 273 and 298 K) are indistinguishable from each other, indicating that the rate coefficienty obtained are not influenced by secondary chemistry. The overall uncertainty in the values of k_1 (using H_2O_2 and HNO_3 precursors for OH) is estimated to be ~7%, which takes into account estimated systematic bias in the SO_2 cross-section at 213.86 nm.

The solid lines are fits to the experimental data according to the Troe formalism for termolecular reactions (Troe, 1983).

$$k_1(T,p) = \frac{k_{1,0}^{N2}\left(\frac{T}{300}\right)^{-n}[M]k_{1,\infty}\left(\frac{T}{300}\right)^{-m}}{k_{1,0}^{N2}\left(\frac{T}{300}\right)^{-n}[M]+k_{1,\infty}\left(\frac{T}{300}\right)^{-m}}F \quad (3)$$

where $k_{1,0}^{N2}$ (cm^6 $molecule^{-2}$ s^{-1}) and $k_{1,\infty}$ (cm^3 $molecule^{-1}$ s^{-1}) are the high-pressure and low-pressure limiting rate coefficients, respectively; *T* is the temperature (K), [M] is the molecular density (molecule cm^{-3}), *n* and *m* are temperature exponents. The broadening factor *F* (which accounts for the lower rate coefficients measured in the fall-off regime than predictions by the Lindemann-Hinshelwood mechanism) is expressed as

$$\log F = \frac{\log F_C}{1+\left[\log\left(\frac{k_{1,0}^{N2}\left(\frac{T}{300}\right)^{-n}[M]}{k_{1,\infty}\left(\frac{T}{300}\right)^{-m}}\right)/N\right]^2} \quad (4)$$

where N = 0.75-1.27logF_C and F_C is the broadening factor at the centre of the fall-off curve.

In order to reduce the number of variables when fitting, we assume that $k_{1,\infty}$ is independent of the temperature (m = 0). This assumption is reasonable as *m* is expected to be small and the data at high pressures (neither in this work nor in the literature) do not accurately define this parameter. If all remaining variables ($k_{1,0}^{N2}$, $k_{1,\infty}$, F_C and *m*) are allowed to float, the least-squares

https://doi.org/10.5194/acp-2021-1074
Preprint. Discussion started: 9 February 2022

Atmospheric Chemistry and Physics Discussions

optimization using Eq. (3) and Eq. (4) gives $k_{1,0}^{N2}$ = 3.03×10^{-31} cm^6 molecule^{-2} s^{-1}, $k_{1,\infty}$ = 2.00×10^{-12} cm^3 molecule^{-1} s^{-1}, F_C = 0.58 and n = 4.10 (see **Table 2,** Method 1). These parameters, with an R^2 correlation coefficient of over 0.994, accurately reproduce all our measurements in N_2 bath gas, as shown in **Fig. 9**.

As the range of temperatures encountered in the Earth's atmosphere is relative narrow, temperature-dependent forms of F_C are no longer widely used in IUPAC evaluations, though a value of F_C = exp(-T/472) is still recommended for the reaction between OH and SO_2. We therefore also explored the effect of setting F_C to exp(-T/472) and allowing a smaller set of variables, $k_{1,0}^{N2}$, $k_{1,\infty}$ and n, to float while fitting. This results in a 20 % higher $k_{1,0}^{N2}$ of 3.60×10^{-31} cm^6 molecule^{-2} s^{-1}, an almost identical value of $k_{1,\infty}$ = 2.01×10^{-12} cm^3 molecule^{-1} s^{-1} and n = 2.86 (**Table 2**, method 2). In addition, we examined the effect of varying the parameter m (i.e. making $k_{1,\infty}$ temperature dependent) while F_C was varied (but kept temperature independent). In this case we obtained $k_{1,\infty}$ = 2.03×10^{-12} cm^3 molecule^{-1} s^{-1} with m = -0.18 and a lower value of $k_{1,0}^{N2}$ (2.82×10^{-31} cm^6 molecule^{-2} s^{-1}) with n = 4.34 (**Table 2**, Method 3).

The quality of the fits obtained using Methods 1, 2 or 3 are very similar (see values for the residual standard deviation and correlation coefficients in **Table 2**), as highlighted in **Fig. S1** of the Supplementary Information where pressure and temperature dependent values of k_1 calculated using all three methods are plotted along with the experimental data. We also show in **Fig. S2** a plot of k_1 derived using each method versus altitude with the appropriate altitude dependent change in temperature and pressure for a standard atmosphere. Clearly, Methods 1 and 3, which have the lowest residual standard deviations are in excellent agreement throughout the atmosphere, with slight differences to Method 2 in the stratosphere. Interestingly, the pressure and temperature dependence of k_1 cancel each other in the lowest 10 km of the Earth's atmosphere, so that k_1 is roughly constant at a value close to 1×10^{-12} cm^3 molecule^{-1} s^{-1}.

For the purpose of modelling the Earth's atmosphere, it is more important to ensure that the data at low and intermediate pressures and temperatures are correctly reproduced by the parameterization, with correct definition of $k_{1,\infty}$ of secondary importance. For this reason, we have chosen to use the parameters derived in Method 1 to calculate k_1 and to compare with previous datasets and evaluations.

3.3. Comparison with previous parametrizations for N_2 bath-gas

Despite the importance of the title reaction in the atmosphere there were no prior temperature dependent measurements of k_1 in atmospherically relevant bath-gases. In experiments designed to define $k_{1,0}$, low-pressure flow-tube studies (Leu, 1982; Lee et al., 1990) measured values of k_1 at N_2 pressures between 0.6 and 5 Torr. In order to access $k_{1,\infty}$, (Fulle et al., 1999) performed experiments in He bath-gas at pressures up to 96 bar. However, under all experimental conditions investigated so far, the title reaction is still in the fall-off regime and neither high- nor low- pressure limits for the title reactions have been attained directly, experimentally.

In **Table 2** we compare our values of k_0, k_∞, F_C, n and m obtained in N_2 with the IUPAC and NASA expressions (both for N_2 bath-gas), as well as parameterizations reported by previous studies (Wine et al., 1984; Fulle et al., 1999; Blitz et al., 2017b),

https://doi.org/10.5194/acp-2021-1074
Preprint. Discussion started: 9 February 2022

Atmospheric Chemistry and Physics Discussions

which were mostly based on temperature-dependent measurements in other bath gases. The value of $k_{1,0}^{N2}$ derived in this work (Method 1) is close to those of 2.8×10^{-31} and 2.9×10^{-31} cm^6 molecule^{-2} s^{-1} preferred by IUPAC and NASA, respectively, and the current value of k_∞ is identical to the recommendation of 2.0×10^{-12} cm^3 molecule^{-1} s^{-1} by IUPAC; The current value of n is equal to the vlue of 4.1 used in the NASA expression, but larger than the IUPAC preferred value of 2.6 unless we adopt the temperature dependent value for F_C which IUPAC uses. In that case our value of n = 2.86 is close to that of IUPAC. This is readily understood as our value of F_C = 0.58 is very close to the "standard" NASA value of F_C = 0.6.

Figure 10 provides a comparison between our data-points and parameterization (Method 1) with the literature data at 298 K obtained in N_2 (Leu, 1982; Lee et al., 1990; Paraskevopoulos et al., 1983; Wine et al., 1984) and with the IUPAC and NASA evaluations. In **Fig. S3** of the Supplementary Information we plot the ratios of literature rate constants obtained at 298 K in N_2 to our parameterisation. Also presented in **Fig. 10** is a modified parameterisation based on Blitz et al. (2017b) (master equation analyses of the (Paraskevopoulos et al., 1983) and (Wine et al., 1984) data sets). Note that the curve plotted cannot be reproduced using the parameters listed in **Table 2** of Blitz et al. (2017b) but is based on data (listed in Table 2) sent in a personal communication with Mark Blitz and takes care of various errors in the published analysis. The comparison in N_2 is restricted to 298 K as, prior to this study, all temperature dependent studies were performed in SiF_6, He or Ar.

In the common pressure range, (in the fall-off regime) our values of k_1 agree very well with those reported by Paraskevopoulos et al. (1983) and Wine et al. (1984). The fall-off curves described by our parameterization and the IUPAC and NASA recommendations are very similar over this pressure range, though our parameterization gives a slightly higher value of k_1 (298 K, 1 atm) (1.04×10^{-12} cm^3 molecule^{-1} s^{-1}) than those proposed by IUPAC and NASA (9.38 and 9.50×10^{-13} cm^3 molecule^{-1} s^{-1}, respectively). In this context, we note that the value of $k_{1,\infty}$ chosen by IUPAC was a compromise between the rate coefficients measured at extended pressures of He by Fulle et al. (1999) and the data from Blitz et al. (2017a). These values are however very divergent with $k_{1,\infty} = 3.6\times10^{-12}$ cm^3 molecule^{-1} s^{-1} and $k_{1,\infty} = 7.5 \times 10^{-13}$ cm^3 molecule^{-1} s^{-1} , respectively. We show below, that at 220 K our value of k_1 in 400 Torr of N_2 ($13.71 \pm 0.41 \times 10^{-13}$ cm^3 molecule^{-1} s^{-1}) while clearly still in the fall-off regime, is a factor of two larger than the value of $k_{1,\infty} = 7.5 \times 10^{-13}$ cm^3 molecule^{-1} s^{-1} reported by Blitz et al. (2017a). Similarly, our value obtained using 351 nm photolysis of HONO as OH source (i.e. when SO_2 excitation can be ruled out) results in $k_1 = 8.44\pm0.19 \times 10^{-13}$ cm^3 molecule^{-1} s^{-1} in 295 Torr of N_2, again above the high-pressure limit reported by Blitz et al. (2017a). Blitz et al. (2017b) suggested that the larger literature values of $k_{1,\infty}$ available at the time of their study were a result of photo-excitation of SO_2. However, our results have clearly shown that a) such effects are absent in N_2 bath-gas when using 248 nm photolysis to generate OH and b) can be ruled out when working at 351 nm (see above). The excellent agreement between the present rate coefficients and those obtained previously in N_2 at 298 K (Paraskevopoulos et al., 1983; Wine et al., 1984) using completely different OH generation methods strongly suggest that data in N_2 are unaffected by such processes, though we cannot rule out that they are the cause of the large values of $k_{1,\infty}$ obtained by Fulle et al. (1999) in He. The present and previous datasets in N_2 indicate that $k_{1,\infty}$ is close to 2×10^{-12} cm^3 molecule^{-1} s^{-1}.

https://doi.org/10.5194/acp-2021-1074
Preprint. Discussion started: 9 February 2022

Atmospheric Chemistry and Physics Discussions

At lower pressures, the IUPAC, NASA and the present parameterizations capture the flow-tube measurements at 1 Torr and above (Leu, 1982; Lee et al., 1990), whereas at the very lowest pressures, there is substantial deviation. This is likely to reflect bias in the flow-tube data caused e.g. by wall-losses of OH and large corrections for axial diffusion.

3.4. Influence of water vapour on k_1

To examine the effects of water vapour (e.g. as a 3rd-body quenching agent) on the kinetics of the title reaction, k_1 was measured in N_2-H_2O mixtures at 273, 298 and 333 K. A total pressure of 50 Torr (N_2 + H_2O) was chosen for these experiments as sensitivity to a potential increase in k_1 through the presence of water is highest at conditions far from $k_{1,\infty}$. As described in Section 2.2, both SO_2 (at 213.856 nm) and H_2O (at 184.95 nm) were monitored online by optical absorption. The large absorption cross section of HNO_3 at 184.95 nm (1.61×10^{-17} cm^2 molecule^{-1}) (Dulitz et al., 2018) would hinder the accurate determination of the H_2O concentration and H_2O_2 was therefore used as the OH precursor in all measurements in N_2-H_2O bath-gas. The molar H_2O mixing ratio in N_2 (x_{H_2O}) was varied up to 0.2 for measurements at 298 and 333 K, and up to 0.05 at 273 K to avoid condensation of water in the reactor and optical absorption cells. The results are summarized in **Table S2**, and measured values of k_1 are plotted versus x_{H_2O} in **Fig. 11** in which k_1 is seen to increase with the water content of the bath gas, indicating that H_2O is a more efficient third-body quencher than N_2 for the title reaction. This is illustrated in **Fig. 12** where we plot the fall-off curves for k_1 in N_2 and H_2O bath-gases. We note that, as for examining the water-vapour effect in the OH + NO_2 reaction (Amedro et al., 2020), continuous, in-situ measurement of the SO_2 concenration is critical to obtaining the correct result as SO_2 concentrations (i.e. optical density at 213.86 nm) decreased when H_2O was added to the flowing H_2O_2 / SO_2 / N_2 mixture. This presumably reflects losses of SO_2 on the glass surfaces of the apparatus on which H_2O would have been adsorbed.

To evaluate the role of water on the rate coefficient of the title reaction, a parameterisation of the 3rd-body effect of H_2O is required and we adopt the approach used in Amedro et al. (2020) for the OH + NO_2 reaction.

Extending Eq. (3), k_1 in N_2-H_2O mixture can be expressed by

$$k(T,p) = \frac{(x_{N_2}k_{1,0}^{N2}\left(\frac{T}{300}\right)^{-n} + x_{H_2O}k_{1,0}^{H2O}\left(\frac{T}{300}\right)^{-o})[M]k_{1,\infty}\left(\frac{T}{300}\right)^{-m}}{x_{N_2}k_{1,0}^{N2}\left(\frac{T}{300}\right)^{-n} + x_{H_2O}k_{1,0}^{H2O}\left(\frac{T}{300}\right)^{-o})[M] + k_{1,\infty}\left(\frac{T}{300}\right)^{-m}}F \quad (5)$$

where x_{H_2O} and x_{N_2} are the mole fraction of H_2O and N_2, $k_{1,0}^{H2O}$, is the low-pressure limiting rate coefficients (cm^6 molecule^{-2} s^{-1}) in pure H_2O and o is a dimensionless temperature exponent. The broadening factor F is then:

$$\log F = \frac{\log F_C}{1+\left[log\left(\frac{x_{N_2}k_{1,0}^{N2}\left(\frac{T}{300}\right)^{-n} + x_{H_2O}k_{1,0}^{H2O}\left(\frac{T}{300}\right)^{-o})[M]}{k_{1,\infty}\left(\frac{T}{300}\right)^{-m}}\right)/N\right]^2} \quad (6)$$

Here, the low-pressure limiting rate coefficients in pure N_2 and pure H_2O are linearly mixed and the same value of F_C is assumed for simplification. By inputting the values of $k_{1,0}^{N2}$, $k_{1,\infty}$, F_C and n listed in **Table 2** (Method 1), a multivariate, least-squares fit (solid lines in **Fig. 9**) results in $k_{1,0}^{H2O}$ = 1.65×10^{-30} cm^6 molecule^{-2} s^{-1} and o = 4.90, indicating that H_2O, as a third-body collider, is at least five times more efficient than N_2.

https://doi.org/10.5194/acp-2021-1074
Preprint. Discussion started: 9 February 2022


Atmospheric Chemistry and Physics Discussions

We also consider the use of different values of F_C for N_2 and H_2O, which may be more appropriate for bath-gases with distinctly different properties (Burke and Song, 2017) and adopted for the OH+NO_2 reaction in He-H_2O mixtures (Amedro et al., 2020). In the present case, however, F_C for N_2 is already close to 0.6, so the differences are expected to be small and the use of the more complex expression for the purpose of atmospheric modelling of the reaction is not warranted. This is detailed in the Supplementary Information.

3.5. Atmospheric modelling of the OH + SO_2 reaction including the effect of water vapour

The chemistry and climate simulation model used is EMAC (ECHAM-MESSy) which uses the 5th generation European Centre Hamburg general circulation model (ECHAM5, Roeckner et al. (2006)) as core atmospheric general circulation model (Jöckel et al., 2006; Jöckel et al., 2010). In this study we used EMAC (ECHAM5 version 5.3.02, MESSy version 2.55.0) at T63L47MA-resolution, i.e. with a spherical truncation of T63 (~1.8 by 1.8 degrees in latitude and longitude) with 47 vertical hybrid terrain following-pressure levels up to 0.01 hPa. The model was weakly nudged in spectral space, applying Newtonian relaxation of the parameters temperature, vorticity, divergence and surface pressure to meteorological reanalysis data (Jeuken et al., 1996). The model set-up is identical to the simulation RED presented in Reifenberg et al. (2021) where the model was evaluated against an aircraft campaign over Europe. In addition, the model has been evaluated on many occasions (Pozzer et al., 2012a; Pozzer et al., 2012b; Yan et al., 2019). For additional references, see http://www.messy-interface.org. As in Reifenberg et al. (2021), EMAC was used in a chemical-transport model (Deckert et al., 2011) without feedbacks between photochemistry, radiation and atmospheric dynamics. In this work, we performed three identical simulations for the year 2019 but with three different parameterisations of k_1 from this work and from the IUPAC and NASA evaluations panels. For the simulations we assume that O_2 has the same collisional quenching efficiency as N_2 as is for case for nearly all termolecular processes of atmospheric importance.

In **Fig. 13**, we illustrate the impact of H_2O-vapour on the rate coefficient, by plotting the reduction in k_1 at the Earth's surface when setting x_{H2O} to zero relative to using EMAC water-vapour fields. The greatest effect of water vapour on k_1 is found in warm, tropical regions where an average underestimation of the rate coefficient by up to ≈ 5 % is found when $x_{H2O} = 0$. At higher/lower latitudes the effect is diminished and water vapour accounts for only a few percent of the overall rate coefficient at 40 ° N/S. The presence of water vapour does not impact significantly on values of k_1 above the boundary layer.

In **Fig. 14** we compare our new parameterisation with preferred parameterisations of the IUPAC and NASA evaluation panels and plot values of k_1(IUPAC) / k_1(This work) and k_1(NASA) / k_1(This work) at different altitudes and latitudes. We parameterized k_1 using the expressions given in this work (Eqn. 5, **Table 2**) and in the latest evaluations of IUPAC (Iupac, 2021) and NASA (Burkholder et al., 2020). k_1(IUPAC) / k_1(This work) varies between 0.88 close to the surface to 0.72 at altitudes above ~ 30 km, whereas k_1(NASA) / k_1(This work) varies between 0.88 at the surface to 0.92 at ~ 30 km. Thus, while both evaluations under-predict k_1 by ≈ 12 % at the surface (partially related to the fact that they do not consider the effects of water-vapour), the NASA parameterisation does well in the lower stratosphere (under-predicting our result by less than 10%)

https://doi.org/10.5194/acp-2021-1074
Preprint. Discussion started: 9 February 2022

Atmospheric Chemistry and Physics Discussions

whereas the IUPAC parameters result in a rate coefficient that is too low by almost 30 %. At high altitudes the divergent rate coefficients recommended by the evaluation panels reflect the choice of experimental data used to derive the low-pressure limiting rate coefficient and its temperature dependence.

As the reaction between OH and SO_2 ultimately results in the formation of H_2SO_4 the atmospheric H_2SO_4 / SO_2 ratio is sensitive to the rate coefficient k_1, with an increase in k_1 resulting in a decrease in SO_2 and an increase in H_2SO_4, thus amplifying the impact. In **Fig. 15** we plot zonally and yearly averaged model values of $\frac{H2SO4}{SO2}(\text{IUPAC})/\frac{H2SO4}{SO2}(\text{this work})$ and $\frac{H2SO4}{SO2}(\text{NASA})/\frac{H2SO4}{SO2}(\text{this work})$. Compared to the parameterization of k_1 in this work, the IUPAC evaluation returns H_2SO_4 / SO_2 ratios that are close to 0.9 at the surface but decrease to 0.7 in the lower to mid stratosphere at low latitudes. Again, the NASA parameterisation performs somewhat better, though here we also find an underestimation of the H_2SO_4 / SO_2 ratio of between 10 and 20 % throughout most of the atmosphere. The impact on the H_2SO_4 to SO_2 ratio is thus similar to the change in the rate coefficients so that the expected amplification is not observed in the model. This is related to an increase in the sink term of H_2SO_4 (via nucleation) which counteracts the increase in its production rate.

The modelling studies indicate that use of IUPAC and NASA parameterizations result in very different values of k_1 in some parts of the atmosphere and will result in divergent predictions of partitioning of reactive sulphur gases between SO_2 and H_2SO_4. The present parameterisation, based on precise and accurate temperature dependent measurements in the fall-off regime in N_2 does not rely on potentially erroneous data at very low and very high pressures and is expected to lead to more accurate values of k_1 for modelling the reaction in the Earth's atmosphere both at the surface (where the effect of water-vapour has been considered for the first time) and at the low pressures and temperatures prevalent in the UT-LS region.

5 Conclusions

Rate coefficients for the reaction of SO_2+OH (k_1) in fall-off regime were experimentally determined in a wide range of pressures and temperatures relevant to the atmosphere. More than 100 individual measurements for k_1 were carried out in N_2 and N_2 / H_2O bath gases using pulsed laser photolytic (PLP) generation of OH coupled to real-time detection of OH via laser-induced fluorescence (LIF). The presence of water-vapour was found to enhance the rate coefficient of the title reaction significantly, indicating that H_2O is a more efficient 3rd- body collider than N_2 or O_2 (by a factor of > 5). Based on our comprehensive dataset in the fall-off regime, we derived a new parametrization of the rate coefficient which results in values of k_1 that are larger than those preferred by the IUPAC and NASA panels, leading to a more rapid removal of SO_2 through gas-phase oxidation than previously assumed and thus to an underestimation of the H_2SO_4 / SO_2 ratio in nearly all regions of the Earth's atmosphere.

Acknowledgements. We thank Dr. Mark. Blitz for communicating revised parameters for the University of Leeds dataset on the title reaction.

https://doi.org/10.5194/acp-2021-1074
Preprint. Discussion started: 9 February 2022

Atmospheric Chemistry and Physics Discussions

Data availability. The rate coefficients measured during this experimental study are listed in the Supplementary information.

Author contributions. The experiments were carried out by WS with assistance from MB and JC. The data analysis was performed by WS. The global modelling was performed by AP. The manuscript was written by WS with assistance from JC and JL.

Competing interests. The authors declare that they have no conflict of interest.

Financial support. The article processing charges for this open access publication were covered by the Max Planck Society.

References

Amedro, D., Bunkan, A. J., Berasategui, M., and Crowley, J. N.: Kinetics of the OH+ NO_2 reaction: rate coefficients (217–333 K, 16–1200 mbar) and fall-off parameters for N_2 and O_2 bath gases, Atmos. Chem. Phys., 19, 10643-10657, doi:/10.5194/acp-19-10643-2019, 2019.

Amedro, D., Berasategui, M., Bunkan, A. J., Pozzer, A., Lelieveld, J., and Crowley, J. N.: Kinetics of the OH+NO_2 reaction: effect of water vapour and new parameterization for global modelling, Atmos. Chem. Phys., 20, 3091-3105, doi:10.5194/acp-20-3091-2020, 2020.

Atkinson, R., Baulch, D. L., Cox, R. A., Crowley, J. N., Hampson, R. F., Hynes, R. G., Jenkin, M. E., Rossi, M. J., and Troe, J.: IUPAC Task Group on Atmospheric Chemical Kinetic Data Evaluation, (http://iupac.pole-ether.fr). Atmos. Chem. Phys., 4, 1461-1738, doi:10.5194/acp-4-1461-2004, 2004.

Badr, O. and Probert, S.: Atmospheric sulphur: trends, sources, sinks and environmental impacts, Applied Energy, 47, 1-67, 1994.

Barnes, I., Bastian, V., Becker, K., Fink, E., and Nelsen, W.: Oxidation of sulphur compounds in the atmosphere: I. Rate constants of OH radical reactions with sulphur dioxide, hydrogen sulphide, aliphatic thiols and thiophenol, J. Atmos. Chem., 4, 445-466, doi:10.1007/BF00053845, 1986.

Beilke, S. and Gravenhorst, G.: Heterogeneous SO_2-oxidation in the droplet phase, in: Sulfur in the Atmosphere, Elsevier, 231-239, doi:10.1016/B978-0-08-022932-4.50025-2, 1978.

Bekki, S.: Oxidation of volcanic SO_2: a sink for stratospheric OH and H_2O, Geophys. Res. Lett., 22, 913-916, doi:10.1029/95GL00534, 1995.

Blitz, M. A., Hughes, K. J., and Pilling, M. J.: Determination of the high-pressure limiting rate coefficient and the enthalpy of reaction for OH+SO_2, J. Phys. Chem. A, 107, 1971-1978, 2003.

Blitz, M. A., Salter, R. J., Heard, D. E., and Seakins, P. W.: An experimental study of the kinetics of OH/OD (v= 1, 2, 3)+ SO_2: the limiting high-pressure rate coefficients as a function of temperature, The Journal of Physical Chemistry A, 121, 3175-3183, doi:10.1021/acs.jpca.7b01294, 2017a.

Blitz, M. A., Salter, R. J., Heard, D. E., and Seakins, P. W.: An Experimental and Master Equation Study of the Kinetics of OH/OD+ SO_2: The Limiting High-Pressure Rate Coefficients, The Journal of Physical Chemistry A, 121, 3184-3191, doi:10.1021/acs.jpca.7b01295, 2017b.

Brimblecombe, P.: The global sulfur cycle, in: Treatise on Geochemistry: Second Edition, Elsevier Inc., 559-591, doi:10.1016/B978-0-08-095975-7.00814-7, 2013.

Brown, K. A.: Sulphur in the environment: a review, Environmental Pollution Series B, Chemical and Physical, 3, 47-80, doi:10.1016/0143-148X(82)90042-8, 1982.

Burke, M. P. and Song, R.: Evaluating mixture rules for multi-component pressure dependence: H+O_2 (+M)=HO_2 (+M), Proceedings of the Combustion Institute, 36, 245-253, https://doi.org/10.1016/j.proci.2016.06.068, 2017.

Burkholder, J., Sander, S., Abbatt, J., Barker, J., Cappa, C., Crounse, J., Dibble, T., Huie, R., Kolb, C., and Kurylo, M.: Chemical kinetics and photochemical data for use in atmospheric studies; evaluation number 19, Jet Propulsion Laboratory, National Aeronautics and Space Administration, 2020.

Cantrell, C. A., Zimmer, A., and Tyndall, G. S.: Absorption cross sections for water vapor from 183 to 193 nm, Geophys. Res. Lett., 24, 2195-2198, 1997.

Castleman Jr, A. and Tang, I.: Kinetics of the association reaction of SO_2 with the hydroxyl radical, J. Photochem., 6, 349-354, doi:10.1016/0047-2670(76)85073-3, 1976.

Cox, R.: Photochemical oxidation of atmospheric sulphur dioxide, Philosophical Transactions of the Royal Society of London. Series A, Mathematical and Physical Sciences, 290, 543-550, doi:10.1098/rsta.1979.0013, 1979.

Cox, R. and Sheppard, D.: Reactions of OH radicals with gaseous sulphur compounds, Nature, 284, 330-331, doi:10.1038/284330a0, 1980.

Davis, D., Ravishankara, A., and Fischer, S.: SO_2 oxidation via the hydroxyl radical: atmospheric fate of HSOx radicals, Geophys. Res. Lett., 6, 113-116, doi:10.1029/GL006i002p00113, 1979.

Deckert, R., Jockel, P., Grewe, V., Gottschaldt, K. D., and Hoor, P.: A quasi chemistry-transport model mode for EMAC, Geoscientific Model Development, 4, 195-206, 2011.

Dulitz, K., Amedro, D., Dillon, T. J., Pozzer, A., and Crowley, J. N.: Temperature-(208–318 K) and pressure-(18–696 Torr) dependent rate coefficients for the reaction between OH and HNO_3, Atmos. Chem. Phys., 18, 2381-2394, doi:10.5194/acp-18-2381-2018, 2018.

Feichter, J., Kjellström, E., Rodhe, H., Dentener, F., Lelieveldi, J., and Roelofs, G.-J.: Simulation of the tropospheric sulfur cycle in a global climate model, Atmos. Env., 30, 1693-1707, doi:10.1016/1352-2310(95)00394-0, 1996.

Fulle, D., F. Hamann, H., and Hippler, H.: The pressure and temperature dependence of the recombination reaction $HO+SO_2+M \rightarrow HOSO_2+M$, Phys. Chem. Chem. Phys., 1, 2695-2702, doi:10.1039/A901596E, 1999.

Heckendorn, P., Weisenstein, D., Fueglistaler, S., Luo, B. P., Rozanov, E., Schraner, M., Thomason, L. W., and Peter, T.: The impact of geoengineering aerosols on stratospheric temperature and ozone, Environ. Res. Lett., 4, 045108, doi:10.1088/1748-9326/4/4/045108, 2009.

Huang, H.-L. and Chao, W.: Kinetics of a Criegee intermediate that would survive high humidity and may oxidize atmospheric SO_2, Proceedings of the National Academy of Sciences, 112, 10857-10862, doi:10.1073/pnas.1513149112, 2015.

IUPAC Task Group on Atmospheric Chemical Kinetic Data Evaluation, (Ammann, M., Cox, R.A., Crowley, J.N., Herrmann, H., Jenkin, M.E., McNeill, V.F., Mellouki, A., Rossi, M. J., Troe, J. and Wallington, T. J.). Last access Sept. 2021: http://iupac.pole-ether.fr/index.html.

Izumi, K., Mizuochi, M., Yoshioka, M., Murano, K., and Fukuyama, T.: Redetermination of the rate constant for the reaction of hydroxyl radicals with sulfur dioxide, Env. Sci. Tech., 18, 116-118, doi:10.1021/es00120a014, 1984.

Jeuken, A. B. M., Siegmund, P. C., Heijboer, L. C., Feichter, J., and Bengtsson, L.: On the potential of assimilating meteorological analyses in a global climate model for the purpose of model validation, J. Geophys. Res. -Atmos., 101, 16939-16950, 1996.

Jöckel, P., Kerkweg, A., Pozzer, A., Sander, R., Tost, H., Riede, H., Baumgaertner, A., Gromov, S., and Kern, B.: Development cycle 2 of the Modular Earth Submodel System (MESSy2), Geoscientific Model Development, 3, 717-752, 2010.

Jöckel, P., Tost, H., Pozzer, A., Bruhl, C., Buchholz, J., Ganzeveld, L., Hoor, P., Kerkweg, A., Lawrence, M. G., Sander, R., Steil, B., Stiller, G., Tanarhte, M., Taraborrelli, D., Van Aardenne, J., and Lelieveld, J.: The atmospheric chemistry general circulation model ECHAM5/MESSy1: consistent simulation of ozone from the surface to the mesosphere, Atmos. Chem. Phys., 6, 5067-5104, 2006.

Kulmala, M., Laaksonen, A., and Pirjola, L.: Parameterizations for sulfuric acid/water nucleation rates, Journal of Geophysical Research: Atmospheres, 103, 8301-8307, doi:10.1029/97JD03718, 1998.

Lee, Y. Y., Kao, W. C., and Lee, Y. P.: Kinetics of the reaction hydroxyl + sulfur dioxide in helium, nitrogen, and oxygen at low pressure, J. Phys. Chem., 94, 4535-4540, doi:10.1021/j100374a035, 1990.

Lelieveld, J. and Heintzenberg, J.: Sulfate cooling effect on climate through in-cloud oxidation of anthropogenic SO_2, Science, 258, 117-120, doi:10.1126/science.258.5079.117, 1992.

https://doi.org/10.5194/acp-2021-1074
Preprint. Discussion started: 9 February 2022

Lelieveld, J., Roelofs, G. J., Ganzeveld, L., Feichter, J., and Rodhe, H.: Terrestrial sources and distribution of atmospheric sulphur, Philosophical Transactions of the Royal Society of London. Series B: Biological Sciences, 352, 149-158, doi:10.1098/rstb.1997.0010, 1997.

Leu, M. T.: Rate constants for the reaction of hydroxyl with sulfur dioxide at low pressure, The Journal of Physical Chemistry, 86, 4558-4562, doi:10.1021/es00120a014, 1982.

Liu, T., Clegg, S. L., and Abbatt, J. P.: Fast oxidation of sulfur dioxide by hydrogen peroxide in deliquesced aerosol particles, Proceedings of the National Academy of Sciences, 117, 1354-1359, doi:10.1073/pnas.1916401117, 2020.

Manatt, S. L. and Lane, A. L.: A compilation of the absorption cross-sections of SO_2 from 106 to 403 nm, Journal of Quantitative Spectroscopy and Radiative Transfer, 50, 267-276, doi:10.1016/0022-4073(93)90077-U, 1993.

Martin, D., Jourdain, J., and Le Bras, G.: Discharge flow measurements of the rate constants for the reaction $OH+SO_2+He$ and $HOSO_2+O_2$ in relation with the atmospheric oxidation of sulfur dioxide, The Journal of Physical Chemistry, 90, 4143-4147, doi:10.1021/j100408a061, 1986.

Mauldin Iii, R., Berndt, T., Sipilä, M., Paasonen, P., Petäjä, T., Kim, S., Kurtén, T., Stratmann, F., Kerminen, V.-M., and Kulmala, M.: A new atmospherically relevant oxidant of sulphur dioxide, Nature, 488, 193-196, doi:10.1038/nature11278, 2012.

Paraskevopoulos, G., Singleton, D. L., and Irwin, R. S.: Rates of OH radical reactions. The reaction $OH+ SO_2+ N_2$, Chem. Phys. Lett., 100, 83-87, doi:10.1016/0009-2614(83)87267-4, 1983.

Pozzer, A., de Meij, A., Pringle, K. J., Tost, H., Doering, U. M., van Aardenne, J., and Lelieveld, J.: Distributions and regional budgets of aerosols and their precursors simulated with the EMAC chemistry-climate model, Atmos. Chem. Phys., 12, 961-987, 2012a.

Pozzer, A., Zimmermann, P., Doering, U. M., van Aardenne, J., Tost, H., Dentener, F., Janssens-Maenhout, G., and Lelieveld, J.: Effects of business-as-usual anthropogenic emissions on air quality, Atmos. Chem. Phys., 12, 6915-6937, 10.5194/acp-12-6915-2012, 2012b.

Reifenberg, S. F., Martin, A., Kohl, M., Hamryszczak, Z., Tadic, I., Röder, L., Crowley, D. J., Fischer, H., Kaiser, K., Schneider, J., Dörich, R., Crowley, J. N., Tomsche, L., Marsing, A., Voigt, C., Zahn, A., Pöhlker, C., Holanda, B., Krüger, O. O., Pöschl, U., Pöhlker, M., Jöckel, P., Dorf, M., Schumann, U., Williams, J., Curtius, J., Harder, H., Schlager, H., Lelieveld, J., and Pozzer, A.: Impact of reduced emissions on direct and indirect aerosol radiative forcing during COVID–19 lockdown in Europe, Atmos. Chem. Phys. Discuss., 2021, 1-23, 10.5194/acp-2021-1005, 2021.

Roeckner, E., Brokopf, R., Esch, M., Giorgetta, M., Hagemann, S., Kornblueh, L., Manzini, E., Schlese, U., and Schulzweida, U.: Sensitivity of simulated climate to horizontal and vertical resolution in the ECHAM5 atmosphere model, Journal of Climate, 19, 3771-3791, 2006.

Rollins, A. W., Thornberry, T. D., Ciciora, S. J., McLaughlin, R. J., Watts, L. A., Hanisco, T. F., Baumann, E., Giorgetta, F. R., Bui, T. V., and Fahey, D. W.: A laser-induced fluorescence instrument for aircraft measurements of sulfur dioxide in the upper troposphere and lower stratosphere, Atmos. Meas. Tech., 9, 4601-4613, doi:10.5194/amt-9-4601-2016, 2016.

Rufus, J., Stark, G., Smith, P. L., Pickering, J., and Thorne, A.: High-resolution photoabsorption cross section measurements of SO_2, 2: 220 to 325 nm at 295 K, Journal of Geophysical Research: Planets, 108, doi:10.1029/2002JE001931, 2003.

Saltzman, E., Brass, G., and Price, D.: The mechanism of sulfate aerosol formation: Chemical and sulfur isotopic evidence, Geophys. Res. Lett., 10, 513-516, doi:10.1029/GL010i007p00513, 1983.

Schiffman, A., Nelson Jr, D., and Nesbitt, D. J.: Quantum yields for OH production from 193 and 248 nm photolysis of HNO_3 and H_2O_2, The Journal of chemical physics, 98, 6935-6946, doi:10.1063/1.464735, 1993.

Sipilä, M., Berndt, T., Petäjä, T., Brus, D., Vanhanen, J., Stratmann, F., Patokoski, J., Mauldin, R. L., Hyvärinen, A.-P., and Lihavainen, H.: The role of sulfuric acid in atmospheric nucleation, Science, 327, 1243-1246, doi:10.1126/science.1180315, 2010.

Stark, G., Smith, P. L., Rufus, J., Thorne, A., Pickering, J., and Cox, G.: High-resolution photoabsorption cross-section measurements of SO2 at 295 K between 198 and 220 nm, Journal of Geophysical Research: Planets, 104, 16585-16590, doi:10.1029/2002JE001931, 1999.

Stevenson, D., Johnson, C., Collins, W., and Derwent, R.: The tropospheric sulphur cycle and the role of volcanic SO_2, Geological Society, London, Special Publications, 213, 295-305, doi:10.1144/GSL.SP.2003.213.01.18, 2003.

Stutz, J., Kim, E., Platt, U., Bruno, P., Perrino, C., and Febo, A.: UV-visible absorption cross sections of nitrous acid, Journal of Geophysical Research: Atmospheres, 105, 14585-14592, doi:10.1016/S1352-2310(99)00322-2, 2000.

https://doi.org/10.5194/acp-2021-1074
Preprint. Discussion started: 9 February 2022

Troe, J.: Theory of thermal unimolecular reactions in the fall-off range. I. Strong collision rate constants, Berichte der Bunsengesellschaft für physikalische Chemie, 87, 161-169, 1983.

Troe, J.: Toward a Quantitative Analysis of Association Reactions in the Atmosphere, Chem. Rev., 103, 4565-4576, 10.1021/cr020514b, 2003.

Troe, J. and Ushakov, V. G.: Representation of "broad" falloff curves for dissociation and recombination reactions, Zeitschrift für Physikalische Chemie, 228, 1-10, doi:10.1515/zpch-2014-04, 2014.

Vaghjiani, G. L. and Ravishankara, A.: Absorption cross sections of CH_3OOH, H_2O_2, and D_2O_2 vapors between 210 and 365 nm at 297 K, Journal of Geophysical Research: Atmospheres, 94, 3487-3492, doi:10.1029/JD094iD03p03487, 1989.

Vehkamäki, H., Kulmala, M., Napari, I., Lehtinen, K. E., Timmreck, C., Noppel, M., and Laaksonen, A.: An improved parameterization for sulfuric acid–water nucleation rates for tropospheric and stratospheric conditions, Journal of Geophysical Research: Atmospheres, 107, AAC 3-1-AAC 3-10, doi:10.1029/2002JD002184, 2002.

Weisenstein, D. K., Ko, M. K., Sze, N. D., and Rodriguez, J. M.: Potential impact of SO_2 emissions from stratospheric aircraft on ozone, Geophys. Res. Lett., 23, 161-164, doi:10.1029/95GL03781, 1996.

Wine, P., Thompson, R., Ravishankara, A., Semmes, D., Gump, C., Torabi, A., and Nicovich, J.: Kinetics of the reaction OH+ SO_2 + M. fwdarw. $HOSO_2$ + M. Temperature and pressure dependence in the fall-off region, The Journal of Physical Chemistry, 88, 2095-2104, doi:10.1021/j150654a031, 1984.

Wollenhaupt, M., Carl, S., Horowitz, A., and Crowley, J.: Rate coefficients for reaction of OH with acetone between 202 and 395 K, The Journal of Physical Chemistry A, 104, 2695-2705, doi:10.1021/jp993738f, 2000.

Yan, Y. Y., Lin, J. T., Pozzer, A., Kong, S. F., and Lelieveld, J.: Trend reversal from high-to-low and from rural-to-urban ozone concentrations over Europe, Atmos. Env., 213, 25-36, 10.1016/j.atmosenv.2019.05.067, 2019.

https://doi.org/10.5194/acp-2021-1074
Preprint. Discussion started: 9 February 2022

Atmospheric Chemistry and Physics Discussions

555 **Table 1. Temperature and pressure-dependent measurements of k_1**

Reference	Technique	OH generation	[SO_2] measurement	Bath gas (Temp / K)	Pressure (Torr)
Leu (1982)	DF-RF	NO_2 + H	manometric	He (261-414) Ar (298) N_2 (298) O_2 (298) CO_2 (298)	< 10
(Paraskevopoulos et al., 1983)	FP-RA	N_2O/H_2 + *hν*	manometric	N_2 (297)	50−760
(Wine et al., 1984)	FP-RF	H_2O + *hν*	optical absorption	He (300 K) Ar (260, 300, 360 and 420 K) N_2 (300 K) SiF_6 (260, 300, 360 and 420 K)	13−696
(Martin et al., 1986)	DF-EPR DF-MS	NO_2 + H	manometric	He (RT)	1−6
(Lee et al., 1990)	DF-RF	NO_2 + H	manometric	He (280-413) N_2 (298) O_2 (298)	< 6
(Fulle et al., 1999)	FP-LIF	O_3/CH_4 + *hν*	manometric	He (220-400)	760−72000
(Blitz et al., 2003)	LP-LIF	$CHBr_3$ H_2O_2 + *hν*	manometric	He (295-673)	100−200
(Blitz et al., 2017a)	LP-LIF	SO_2 + H_2 + *hν* $(CH_3)_3COOH$ + hν	manometric	He (295)	25−303
This work	LP-LIF	H_2O_2 + *hν* HNO_3 + *hν* HONO + *hν*	optical absorption	N_2 (220-333)	14-742

Notes: DF-RF = discharge flow- resonance fluorescence, FP-RA = flash photolysis- resonance absorption, FP-RF = flash photolysis-resonance fluorescence, DF-EPR-MS = discharge flow-electric paramagnetic resonance / mass spectrometry, FP-LIF = flash photolysis-laser induced fluorescence, LP-LIF = laser flash photolysis-laser-induced fluorescence. RT = room temperature.

https://doi.org/10.5194/acp-2021-1074
Preprint. Discussion started: 9 February 2022

Atmospheric Chemistry and Physics Discussions

Table 2. Parameterisation of k_1 in N_2

	$k_{1,0}$ [1]	n	$k_{1,\infty}$ [2]	m	F_C [3]	RSD [4]	CC [5]	Temp. range (K)
This work Method 1	3.03 (v)	4.10 (v)	2.00 (v)	0 (f)	0.58 (v)	2.27	0.9943	220−333
This work Method 2	3.60 (v)	2.86 (v)	2.01 (v)	0 (f)	exp(-*T*/472) (f)	2.44	0.9928	220−333
This work Method 3	2.82 (v)	4.34 (v)	2.03 (v)	-0.18 (v)	0.59 (v)	2.27	0.9944	220−333
Wine et al. (1984)	5.76	2.57	1.26	0.7	exp(-*T*/388)			260−420
Fulle et al. (1999)	8.3exp(-360/T)	3.3	12exp(-360/T)	0	0.29+0.64exp(-*T*/300)			220−400
Blitz et al. (2017b)[6]	10.6	3.53	0.79	-0.10	0.386exp(-9.3×10^{-5}*T*)			200−600
IUPAC	2.8	2.6	2.0	0	exp(-*T*/472)			200−400
NASA[7]	2.9	4.1	1.7	-0.2	0.6			--

Notes: [1] Units of 10^{-31} cm^6 molecule^{-2} s^{-1}, [2] Units of 10^{-12} cm^3 molecule^{-1} s^{-1}, [3] Temperature (T) in K. [4] RSD (residual standard deviation) for the fitting is defined as $\sqrt{\sum(k_1 - k_{1_p})^2 / N-2}$, k_1 and k_{1_p} are the measured and the fitted rate coefficients and N is the total number of the data points, with the unit of 10^{-14} cm^3 molecule^{-1} s^{-1}. v = allowed to vary during fitting, f = fixed during fitting. [5]CC is the correlation coefficient (R^2). [6] The parameters, which are different from those given in Blitz et al. (2017b) are from a personal communication with Mark Blitz. The parameterization is based on the modified fall-off parameterisation in Troe and Ushakov (2014), details are given in the Supplementary Information. [7] The simplified form of the Troe expression for termolecular reactions used by NASA can be found in the Supplementary Information.

https://doi.org/10.5194/acp-2021-1074
Preprint. Discussion started: 9 February 2022

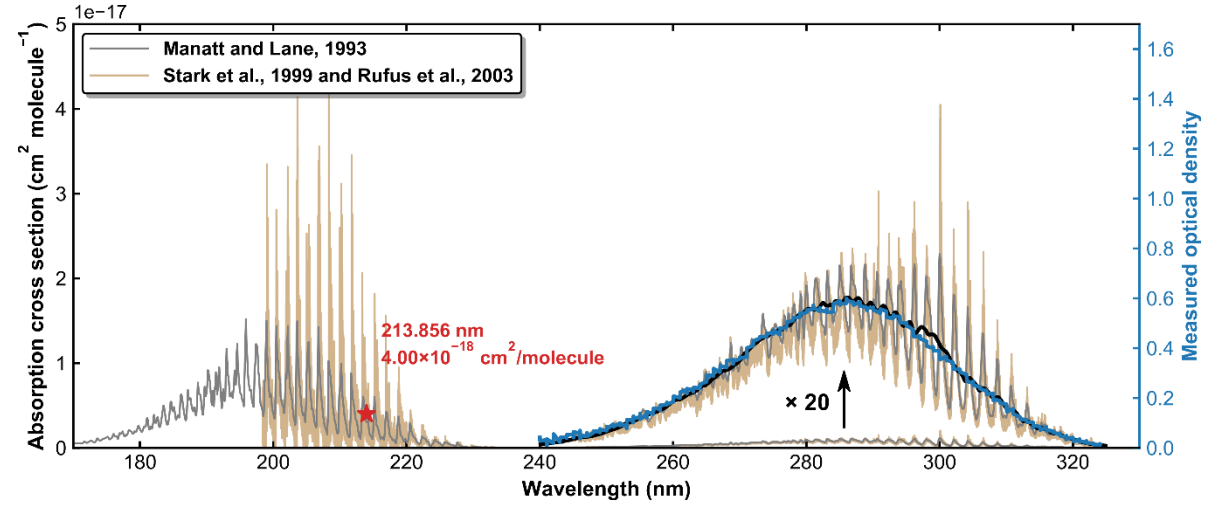

Figure 1. SO_2 absorption spectra reported by Manatt and Lane (1993) and Stark and co-workers (Stark et al., 1999; Rufus et al., 2003). The black line is the result of degrading the resolution in the 240−325 nm region to that of our our optical density measurements (blue line).

https://doi.org/10.5194/acp-2021-1074
Preprint. Discussion started: 9 February 2022

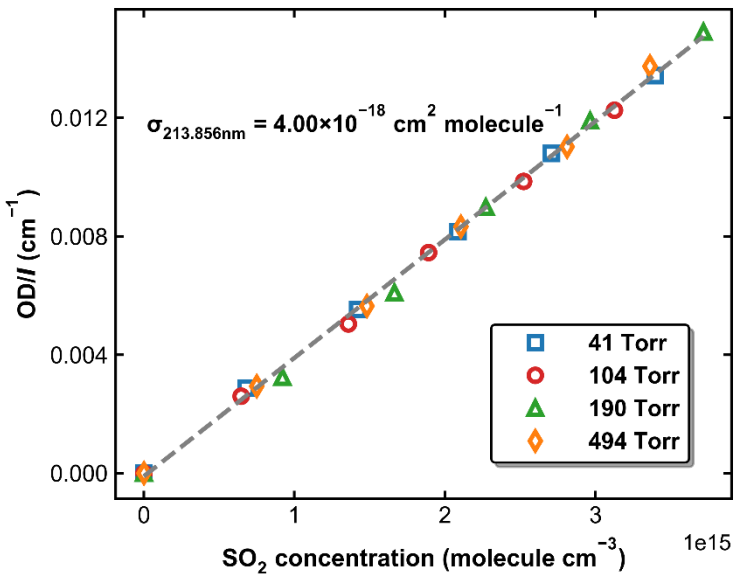

Figure 2. Normalized optical density in the 213.86 nm absorption cell as a function of SO_2 concentration measured using the multi-pass absorption cell. The experiments were performed at 298 K and pressures of 41, 104, 190 and 494 Torr. The grey dashed line is the linear regression, for which the slope is the effective cross section of SO_2 at 213.86 nm.

https://doi.org/10.5194/acp-2021-1074
Preprint. Discussion started: 9 February 2022

Atmospheric Chemistry and Physics Discussions

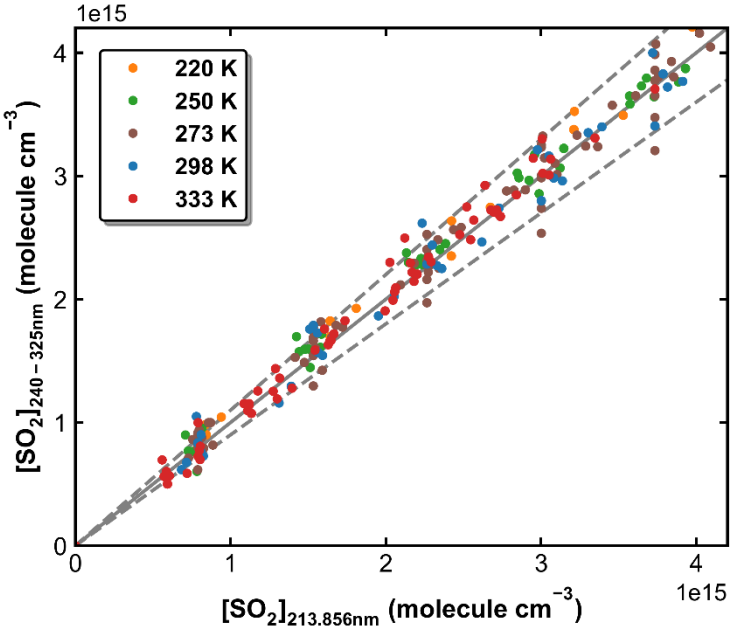

580 **Figure 3.** SO_2 concentrations measured in the experiments at different temperatures using the multi-pass absorption cell upstream of the reactor (*y* axis) and the 213.86 nm absorption cell downstream of the reactor (*x* axis). The solid line represents $y = x$, and the dashed lines are $y = 1.1x$ and $y = 0.9x$.

https://doi.org/10.5194/acp-2021-1074
Preprint. Discussion started: 9 February 2022

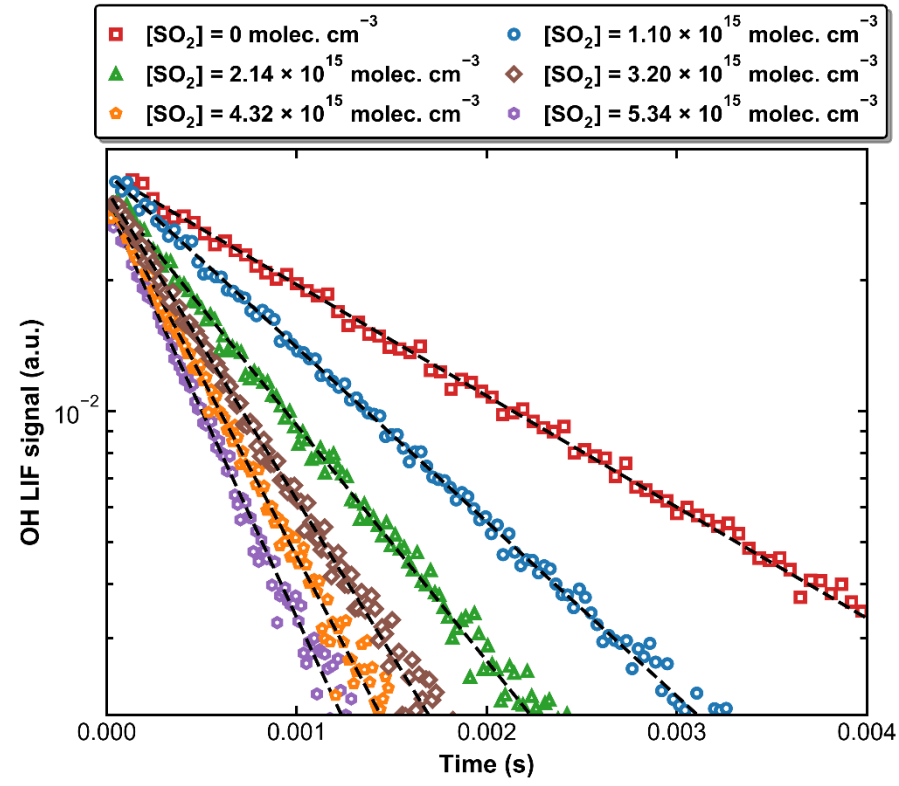

585 **Figure 4.** Exponential decay of OH at 298 K and 59.9 Torr (N_2 bath gas) in the presence of six different SO_2 concentrations. OH was generated by the photolysis of H_2O_2 at 248 nm The black dashed lines are fits using Eqn. (1).

https://doi.org/10.5194/acp-2021-1074
Preprint. Discussion started: 9 February 2022

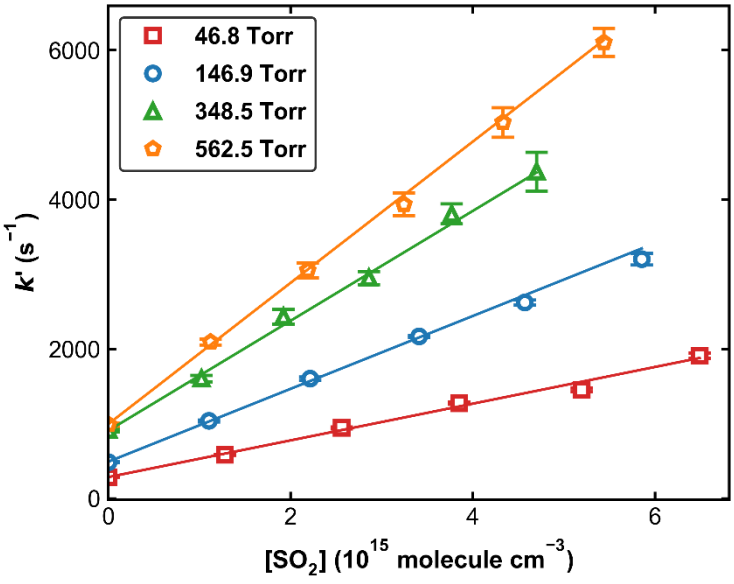

Figure 5. Pseudo-first-order rate coefficients (*k*') as a function of SO_2 concentration ([SO_2]) at four different pressures at 298 K. Error bars represent 2σ statistical uncertainties.The lines are weighted linear regressions.

https://doi.org/10.5194/acp-2021-1074
Preprint. Discussion started: 9 February 2022

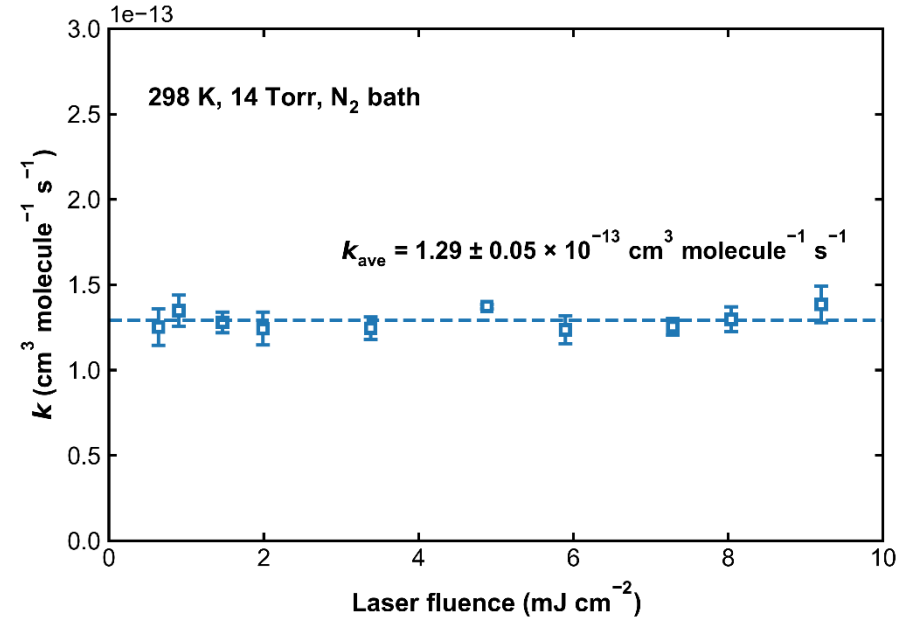

Figure 6. Values of k_1 measured at 298 K and in 14 Torr of N_2 bath gas. The 248 nm laser fluence was varied by a factor of ~ 14. The dashed line represents the average rate coefficient.

595

https://doi.org/10.5194/acp-2021-1074
Preprint. Discussion started: 9 February 2022

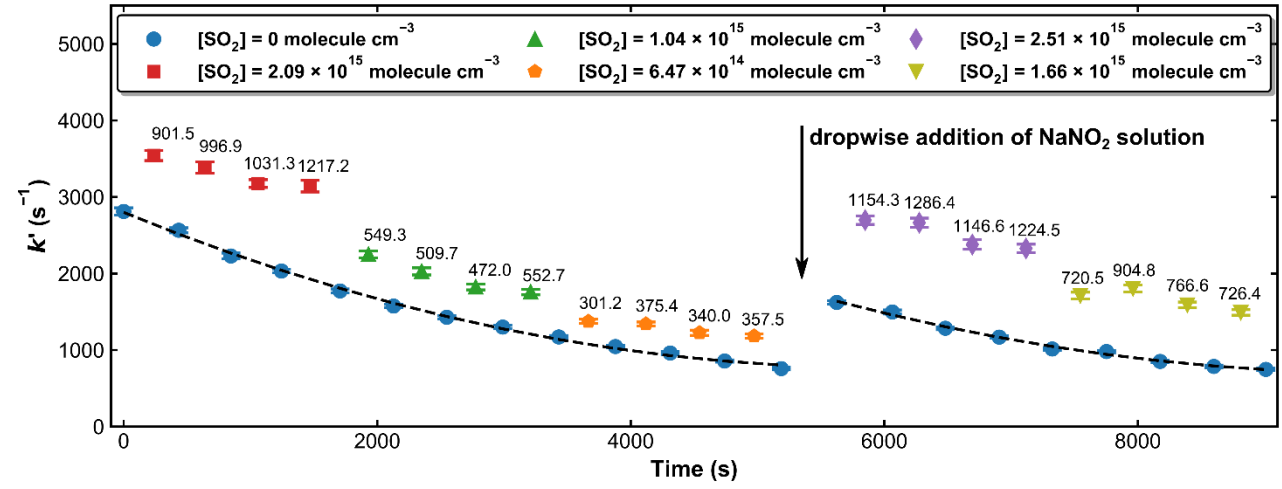

Figure 7. Pseudo-first-order rate coefficients (*k*') at 193.2 Torr and 298 K whereby OH was generated by the 351 nm photolysis of HONO. The time dependent OH decay constants in the absence of SO_2 (blue symbols) were fit to a second-degree polynomial (black dashed lines). The number on the top of each data point when SO_2 is present (red, green, orange, purple and olive coloured symbols), represents the difference in *k*' to that obtained (by interpolation) in the absence of SO_2. A few drops of the $NaNO_2$ solution was re-added after about 90 minutes to maintain OH levels and thus a good signal-to-noise ratio.

https://doi.org/10.5194/acp-2021-1074
Preprint. Discussion started: 9 February 2022

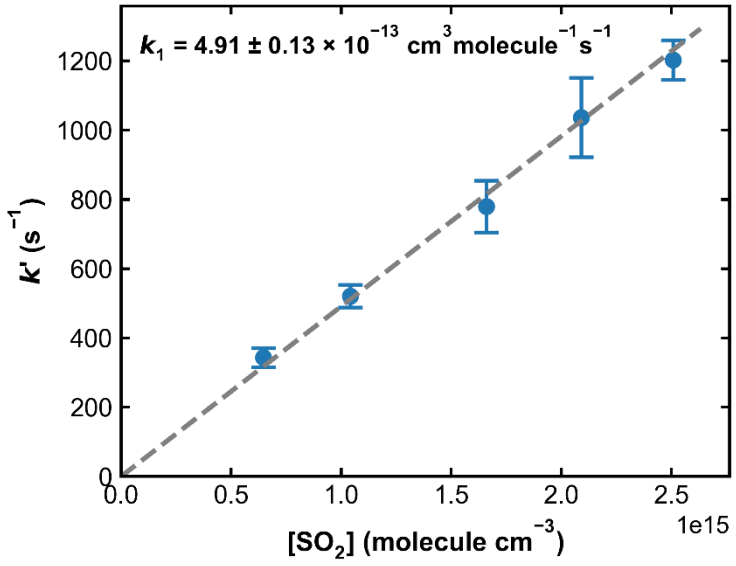

Figure 8. Pseudo-first-order rate coefficients (k') as a function of the SO_2 concentration ([SO_2]) at 193.2 Torr N_2 and 298 K. OH was generated through HONO photolysis at 351 nm. Each data point is an average over four individual measurements and the error bars represent 2σ statistical uncertainties. k_1 was obtained from the slope of the linear regression.

https://doi.org/10.5194/acp-2021-1074
Preprint. Discussion started: 9 February 2022

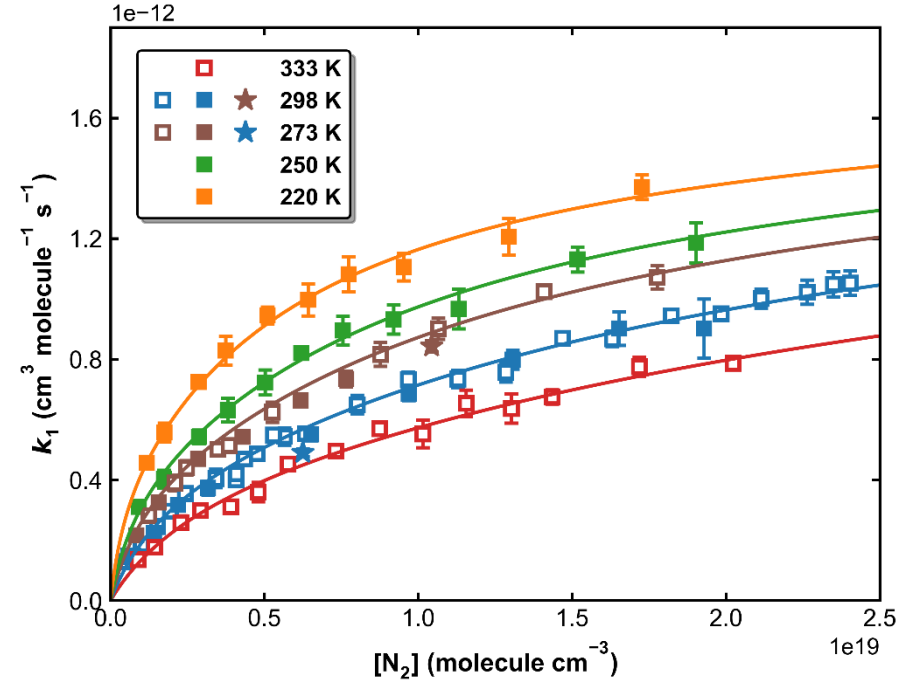

Figure 9. k_1 as a function of N_2 concentration in the fall-off regime at five different temperatures. Open squares, closed squares and stars represent data obtained using H_2O_2, HNO_3 and HONO as OH precursors, respectively. The error bars represent 2σ statistical uncertainties. The solid lines are the fits of the experimental data to Eqn. 3 with $k_0 = 3.03\times10^{-31}$ cm^6 molecule^{-2} s^{-1}, $k_\infty = 2.00\times10^{-12}$ cm^3 molecule^{-1} s^{-1}, n = 4.10, m = 0 and F_C =0.58.

https://doi.org/10.5194/acp-2021-1074
Preprint. Discussion started: 9 February 2022

Atmospheric Chemistry and Physics Discussions

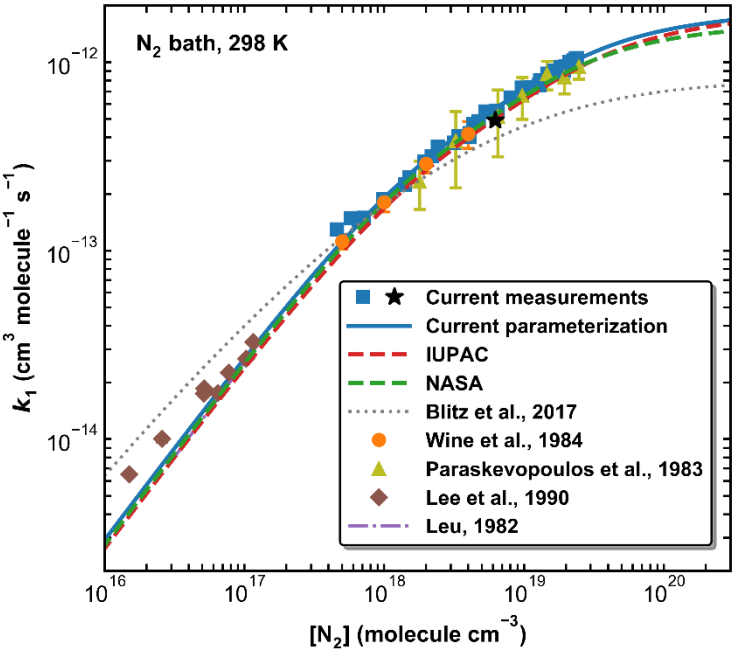

Figure 10. A comparison of previous measurements of k_1 at 298 K (N_2 bath-gas only) with our parameterisation and those of IUPAC, NASA and Blitz et al. (2017b) (see Table 2 for details). The black star represents the measurement using HONO photolysis at 351 nm to generate OH.

https://doi.org/10.5194/acp-2021-1074
Preprint. Discussion started: 9 February 2022

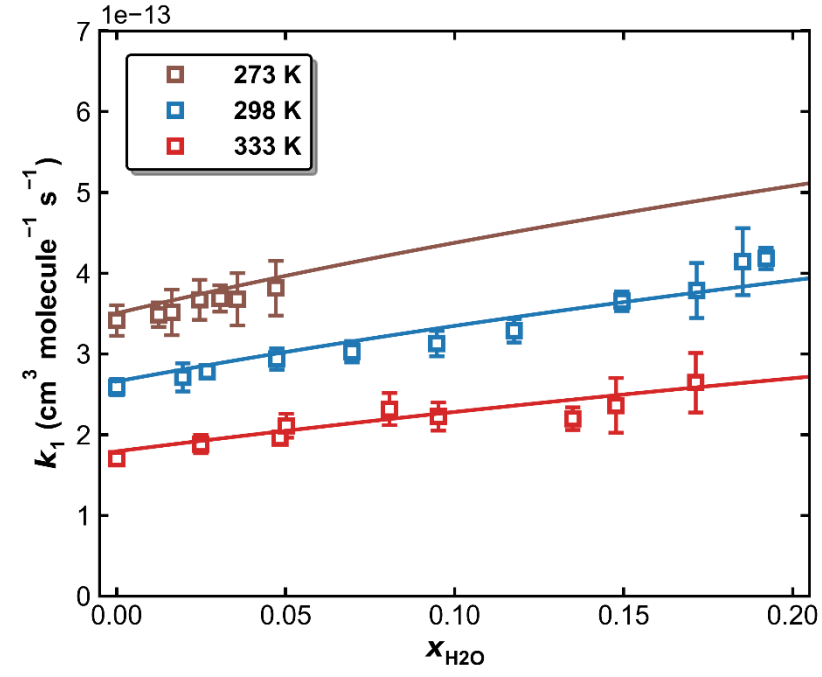

620 **Figure 11.** k_1 as a function of x_{H_2O} in N_2-H_2O bath gas at a total pressure of 50 Torr and different temperatures of 273, 298 and 333 K. The symbols represent measurements and the solid lines are fits to Eqn. (5) and (6) with $k_{1,\infty}$ = 2.00 ×10^{-12} cm^6 molecule^{-2} s^{-1}, $k_{1,0}^{N_2}$ = 3.03 ×10^{-31} cm^6 molecule^{-2} s^{-1}, n = 4.10, m = 0 and F_C = 0.58. The resulting parameters for water are $k_{1,0}^{H_2O}$ = 1.65 ×10^{-30} cm^6 molecule^{-2} s^{-1}, o = 4.90.

https://doi.org/10.5194/acp-2021-1074
Preprint. Discussion started: 9 February 2022

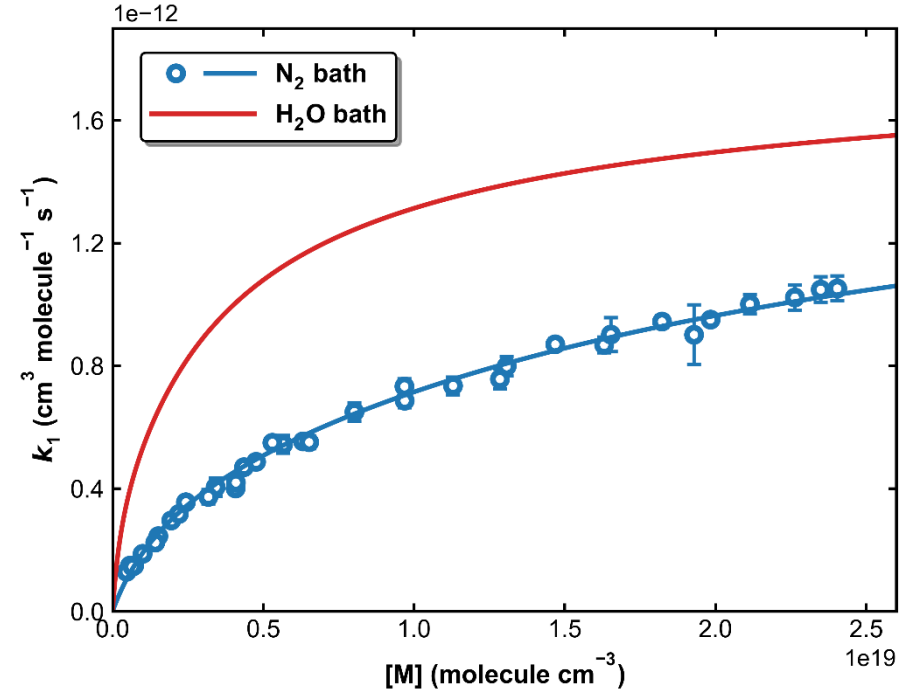

Figure 12. Fall-off curves for k_1 in N_2 and H_2O bath-gases at 298 K. The solid lines are our preferred parameterization with $k_{1,\infty} = 2.0 \times 10^{-12}$ cm^3 $molecule^{-1}$ s^{-1} (independent of bath-gas), $k_{1,0}^{N2} = 3.03\times10^{-31}$ cm^6 $molecule^{-2}$ s^{-1} and $k_{1,0}^{H2O} = 1.65\times10^{-30}$ cm^6 $molecule^{-2}$ s^{-1}, $F_C^{N2} = F_C^{H2O} = 0.58$.

https://doi.org/10.5194/acp-2021-1074
Preprint. Discussion started: 9 February 2022

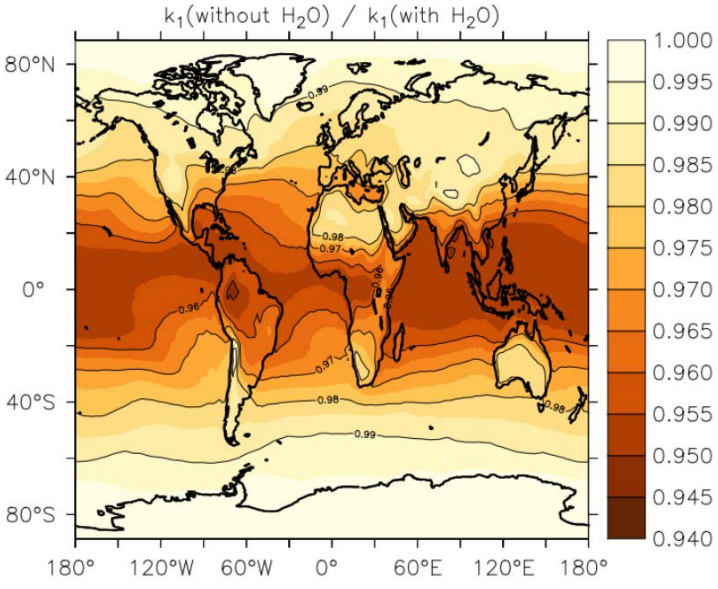

Figure 13. Annual average effect of H_2O on k_1 expressed as the fractional change in the rate coefficient near the Earth's surface when setting the mole fraction of water vapour to zero in Eqn. 5 and 6.

635

https://doi.org/10.5194/acp-2021-1074
Preprint. Discussion started: 9 February 2022

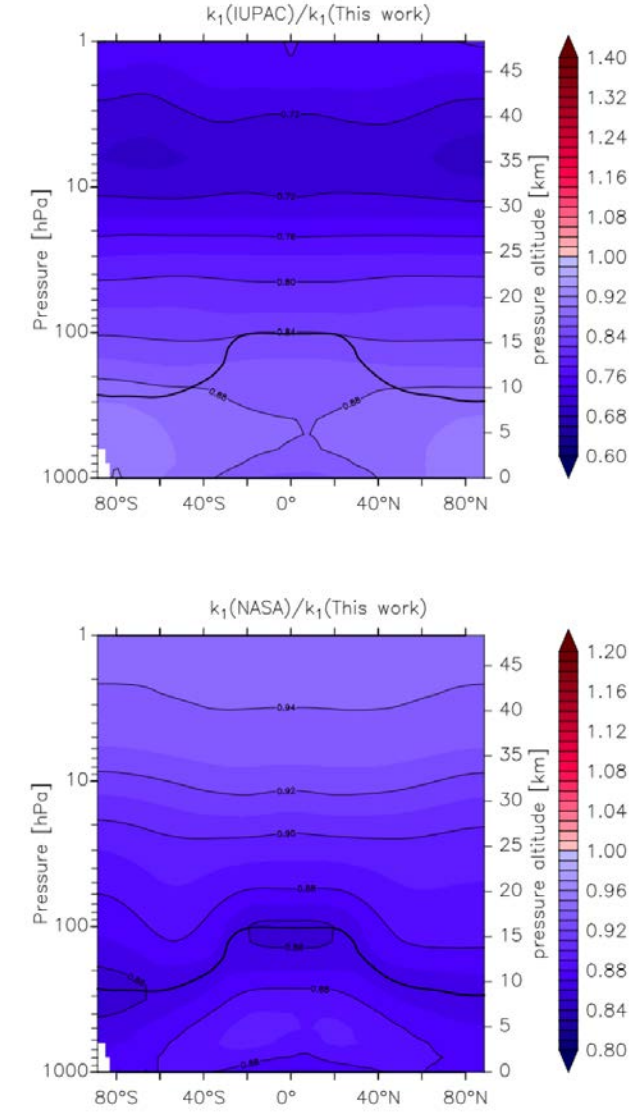

640 **Figure 14.** Global values of $\frac{k_1(\text{IUPAC})}{k_1(\text{This work})}$ (upper panel) and $\frac{k_1(\text{NASA})}{k_1(\text{This work})}$ (lower panel). k_1 was calculated using the parameters from this work and those presently recommended by the IUPAC and NASA data evaluation panels. The relatively thick black line between 300 and 100 hPa represents the mean model tropopause.

https://doi.org/10.5194/acp-2021-1074
Preprint. Discussion started: 9 February 2022

Atmospheric Chemistry and Physics Discussions

645

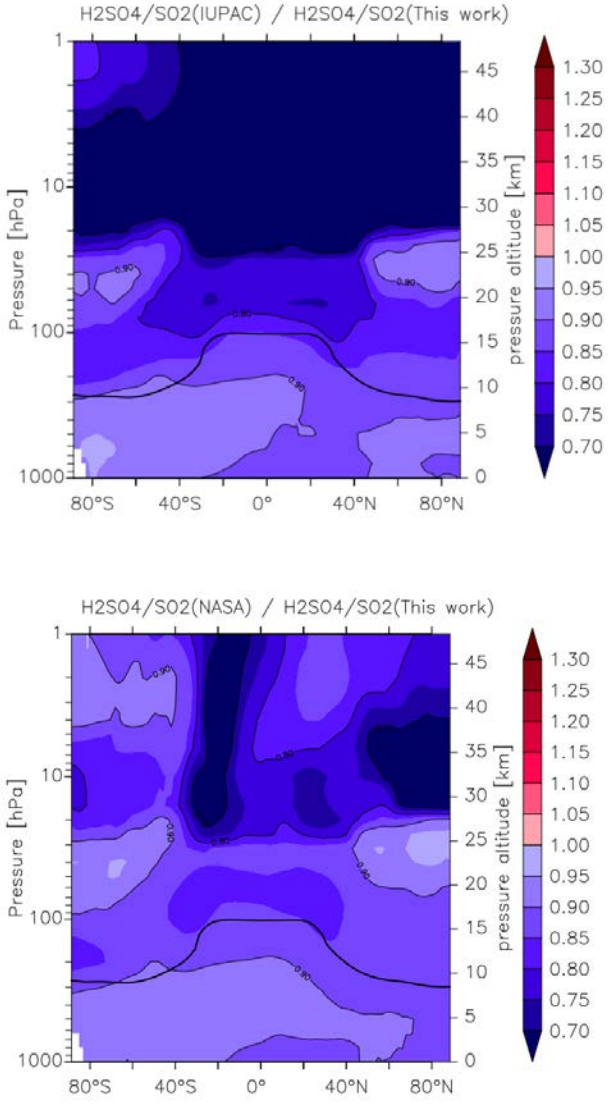

Figure 15. Effect of different parameterisations of k_1 on the global (zonal and yearly averaged) H_2SO_4 to SO_2 ratio. The upper
650 panel plots $\frac{H2SO4}{SO2}$(IUPAC)/$\frac{H2SO4}{SO2}$(this work), the lower panel plots $\frac{H2SO4}{SO2}$(NASA)/$\frac{H2SO4}{SO2}$(this work). The relatively thick black line between 300 and 100 hPa represents the mean model tropopause.